2ND LSA SAF WORKSHOP

INSTITUTO DE METEOROLOGIA

LISBON, PORTUGAL

8-10 MARCH 2006

SESSION 1 – Current and Future Activities

THE EUMETSAT SAF NETWORK AND ITS EVOLUTION

Lorenzo Sarlo

EUMETSAT
Am Kavalleriesand 31D-64295 Darmstadt Germany

The EUMETSAT SAF Network and its Evolution

Lorenzo Sarlo, Lothar Schüller

Programme Preparation & SAF Network Division

EUMETSAT

Outline

- **Deployment of the EUMETSAT SAF Concept**
  - *SAF Objectives and Benefits*
  - *Distributed Application Ground Segment*
- **The SAF Network Organisation**
  - *Roles of SAFs and EUMETSAT*
  - *SAF Life Cycle and Funding*
  - *Data Sources and Dissemination*
- **Current SAF Themes, Projects, and Products**
- **Conclusions**

Deployment of the EUMETSAT SAF Concept

- In 1992 EUMETSAT adopted the concept of a Distributed Application Ground Segment including:
  - *the EUMETSAT Central Facilities in Darmstadt*
  - *and a network of elements known as Satellite Application Facilities (SAF), as specialised development and processing centres.*
- SAFs utilise the **specific expertise** available in EUMETSAT's Member and Cooperating States
- The SAF network **complements** the production of standard meteorological products derived from satellite data at the Central Facilities in Darmstadt, and also distributes user software packages.
- SAFs are developed by **consortia** of organisations from the Member and Cooperating States, and are located at National Meteorological Services in Member states

SAF Objectives and Benefits

SAF OBJECTIVES

- Improving the ability of EUMETSAT Member States to exploit satellite data
- Encouraging the utilisation of existing skills and infrastructure in Member- and Cooperating States for developing geophysical data products and services
- Facilitating cost-effective exploitation by ensuring services are distributed in the most appropriate way
- Fostering development of cooperation with non-Member States and other organisations

The overall objective of a SAF is the provision of operational services, in the context of a cost-effective and synergetic balance between the central and distributed services.

EUMETSAT Satellite Application Facilities
Deployment of the EUMETSAT SAF Concept
SAF Objectives and Benefits
Distributed Application Ground Segment
SAF Network Organization
Roles of SAFs and EUMETSAT
SAF Life Cycle & Funding
Data sources and dissemination
Current SAF Themes, Projects, and Products
Conclusions

SAF Objectives and Benefits (2)

Some major benefits

- Improved information for land use, ecology, disaster monitoring and agricultural forecasting
- Benefits for sea transport, fishing and offshore industries
- Improved data for input to Numerical Weather Prediction
- Availability of user software packages for operational applications

- Improvements to short range forecasting of severe weather hazards
- Benefits to aviation, agriculture, construction, gas, water and electricity industries
- Better understanding of causes and effects of pollution of the upper atmosphere and the depletion of ozone
- Early warning of hazards (precise details for evacuation and alerting of emergency authorities)
- Enhanced data for climate monitoring

Distributed Application Ground Segment

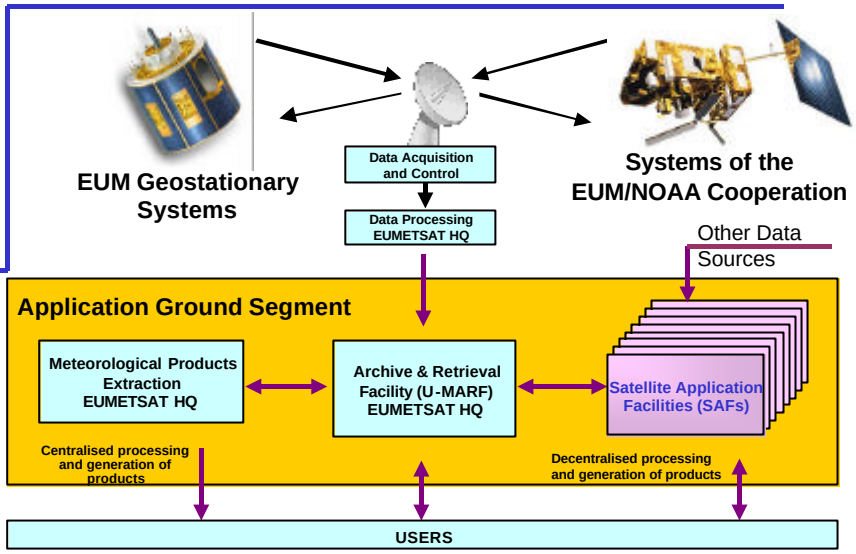

EUMETSAT Satellite Application Facilities
Deployment of the EUMETSAT SAF Concept
SAF Objectives and Benefits
Distributed Application Ground Segment
SAF Network Organization
Roles of SAFs and EUMETSAT
SAF Life Cycle & Funding
Data sources and dissemination
Current SAF Themes, Projects, and Products
Conclusions

SAF Organisation: *Roles of SAFs and EUMETSAT*

SAFs Role

- To undertake on a distributed basis such necessary *R&D and operational activities* that can be carried out in a more effective way than at the EUMETSAT central facility.
- To develop and deliver services/products aimed at enhancing the value and use of data for applications considered to be a common need of all, or the least a majority, of Member States.

EUMETSAT's role

- The Secretariat of EUMETSAT coordinates and monitors the development and operations of the entire SAF Network
- The EUMETSAT STG and AFG review as appropriate the progress of the SAF development and operational phases.

SAF organisation: *Life Cycle and Funding*

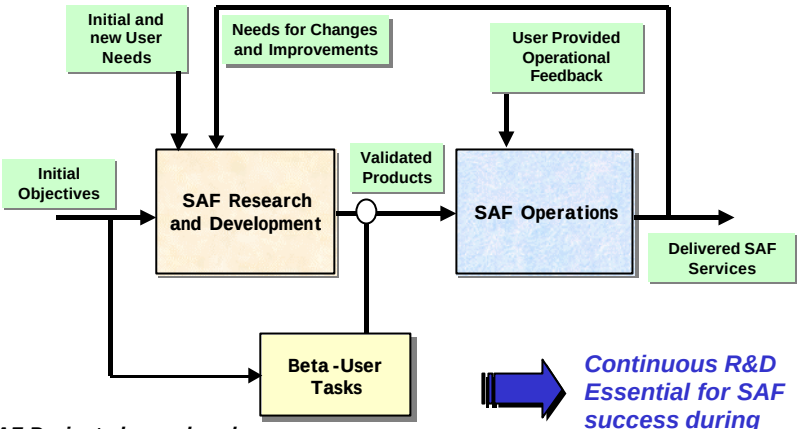

SAF Projects have already stimulated the contribution of few hundreds scientists in many different countries.

Continuous R&D Essential for SAF success during Operations

EUMETSAT Satellite Application Facilities
Deployment of the EUMETSAT SAF Concept
SAF Objectives and Benefits
Distributed Application Ground Segment
SAF Network Organization
Roles of SAFs and EUMETSAT
SAF Life Cycle & Funding
Data sources and dissemination
Current SAF Themes, Projects, and Products
Conclusions

Life Cycle and Funding (2)

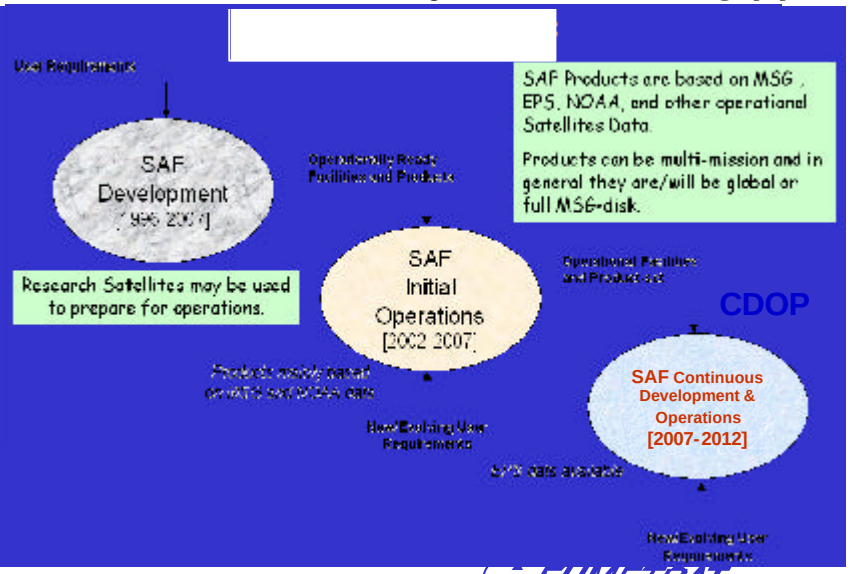

Life Cycle and Funding (3)

- **EUM-SAF Shared Costs Policy**
  - EUM Funding up to 50% for the SAF development phase + dedicated funding for Visiting Scientists
  - EUM Funding up to 75% of operational running costs + dedicated funding for Visiting Scientists
- **Initial Operations Phase (IOP)**
  - In line with EUMETSAT Council decisions, SAF Initial Operations are covered until 2007 within the MSG budget.
- **Continuous Development and Operations Phase 2007-2012**
  - In line with EUMETSAT Council decisions, following IOP, SAF Operations are **covered until 2012** within the EPS budget.
- **Continuous Development and Operations Phase > 2012**
  - To be timely addressed with EUMETSAT Council.

Data Sources and Dissemination

- **SAFs use inputs from meteorological (and other) satellites** in both geostationary and polar orbits
  - during Development phase: *use of data from any suitable satellite system including research missions*
  - during Operations phase: *focus on operational satellites, and in particular EUMETSAT Geostationary and Polar systems*
- **EUMETSAT SAF products are distributed via**
  - The Global Telecommunication System GTS/ Regional Meteorological Data Communication Network RMDCN
  - ***EUMETCast***
  - Internet (FTP)

Data Sources and Dissemination (2)

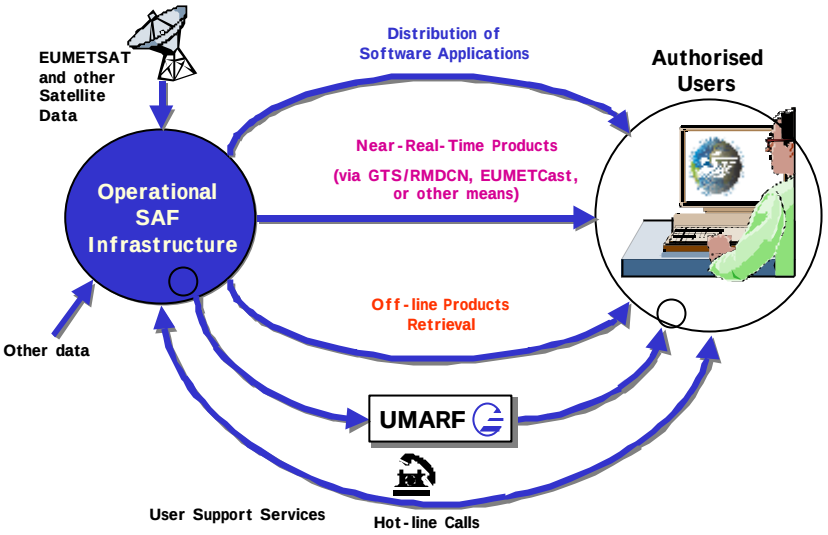

EUMETSAT Satellite Application Facilities
Deployment of the EUMETSAT SAF Concept
SAF Objectives and Benefits
Distributed Application Ground Segment
SAF Network Organization
Roles of SAFs and EUMETSAT
SAF Life Cycle & Funding
Data sources and dissemination
Current SAF Themes, Projects, and Products
Conclusions

Data Sources and Dissemination (3)

- **Distribution of Software to Users**
  - NWC SAF Software Packages
  - NWP SAF Software Libraries
  - elements of the GRAS SAF Software
- **Near-real-time Products services**
  - **Land Surface Analysis SAF**, OSI SAF, O3M SAF, GRAS SAF
- **Off-line Products services**
  - **Land Surface Analysis SAF**, CM SAF, OSI SAF, O3M SAF, GRAS SAF

Current SAF Themes, Projects and Products

- Seven SAFs Projects were approved, related Cooperation Agreements established, and development activities initiated in the period 1997-1999.
- An 8th SAF Theme on *support to Operational Hydrology and Water Management* was approved by Council in November 2002, thus creating a new SAF opportunity.
- A proposal for a new SAF project on this theme, prepared under coordination of the Italian Meteorological Service, was approved by Council in July 2005 and the Project started in September 2005.

SAF in Initial Operations

- **Ocean & Sea Ice SAF**
- **Nowcasting & VSRF SAF**
- **Climate Monitoring SAF**
- **NWP SAF**
- ***Land Surface Analysis SAF***

SAF under Development

- **Ozone Monitoring SAF**
- **GRAS Meteorology SAF**
- ***Support to Operational Hydrology and Water Management SAF***

EUMETSAT Satellite Application Facilities
Deployment of the EUMETSAT SAF Concept
SAF Objectives and Benefits
Distributed Application Ground Segment
SAF Network Organization
Roles of SAFs and EUMETSAT
SAF Life Cycle & Funding
Data sources and dissemination
Current SAF Themes, Projects, and Products
Conclusions

Current SAF Themes, Projects and Products

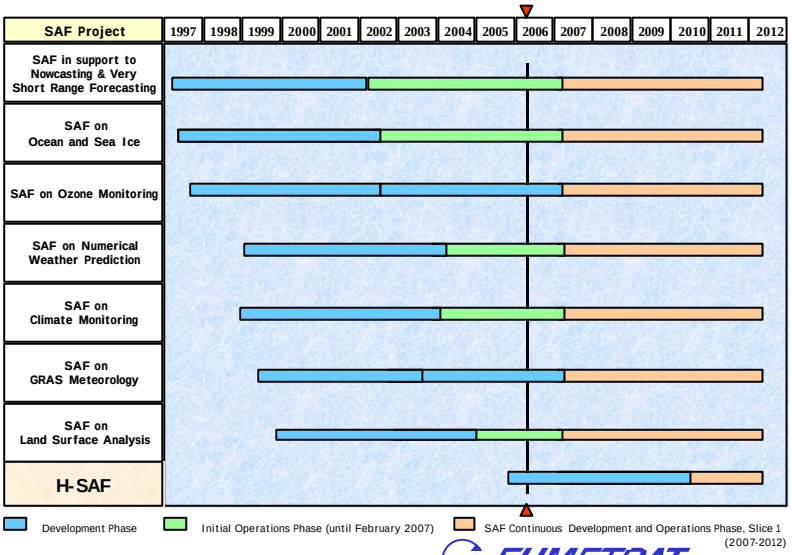

EUMETSAT
EUM/PPS/VWG/06/0033, SAF on Land Surface Analysis Users Workshop, Lisbon, 8-10 March 2006

Land Surface Analysis (LSA) SAF

- Established to increase the benefit from MSG and EPS data related to land, land-atmosphere interaction and biospheric applications
- Host Institute is the Portuguese Institute for Meteorology IM, Lisbon
- The Initial Operations phase of the LSA SAF started in January 2005
- **PRE-Ops Products & Service deployed since 2005**
- ***EUMETCAST in use to disseminate these products***

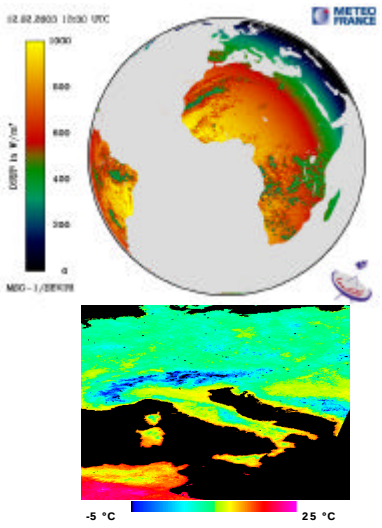

EUMETSAT Satellite Application Facilities
Deployment of the EUMETSAT SAF Concept
SAF Objectives and Benefits
Distributed Application Ground Segment
SAF Network Organization
Roles of SAFs and EUMETSAT
SAF Life Cycle & Funding
Data sources and dissemination
Current SAF Themes, Projects, and Products
Conclusions

Land Surface Analysis SAF (2)

CONTRIBUTION TO GCOS

- Establishment of the WMO Global Climate Observing System (GCOS) in 1992, to
  - Ensure the data needs for climate system monitoring
  - Improve the observing capabilities
  - Integrate observation into useful products
- GCOS focus on Essential Climate Variables
- **The Land SAF is involved in related discussions and workshops and already contribute to prototyping addressing GCOS requirements**

Land Surface Analysis (LSA) SAF (3)

SAF Network contribution to GMES

- Global Monitoring of Environment and Security (GMES)
- establish a European capacity for the provision and use of operational information for Global Monitoring of Environment and Security

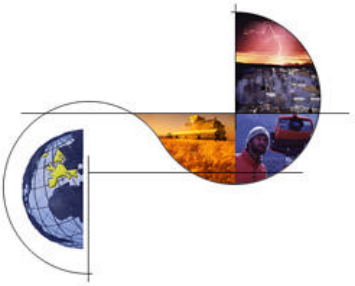

The Land SAF contributes to the GMES GEOLAND Project

and will do as well in the Fast Track Service on Land

EUMETSAT

Land Surface Analysis (LSA) SAF (4)

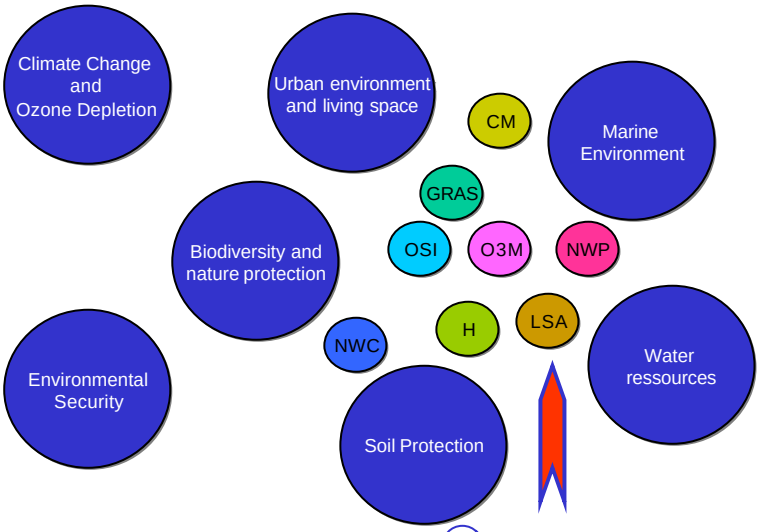

EUMETSAT

Land Surface Analysis (LSA) SAF (5)

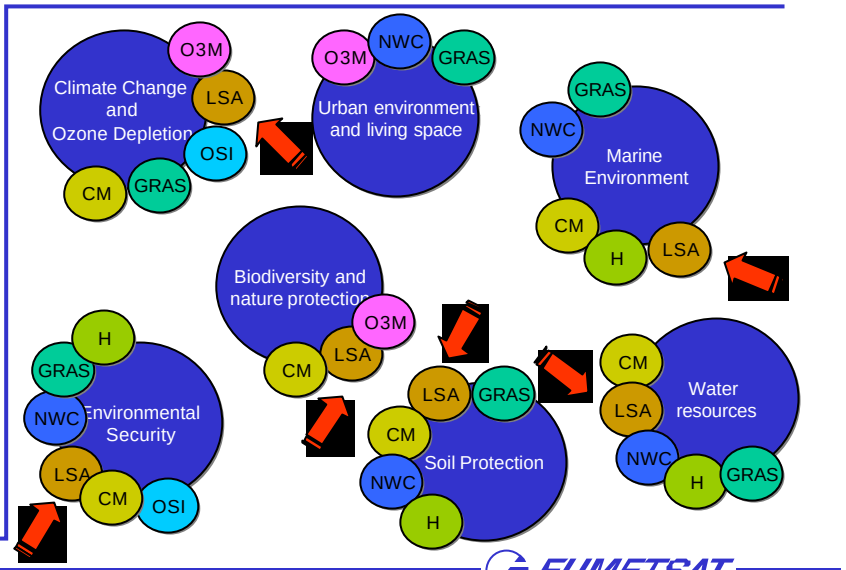

Conclusions

- SAFs are dedicated centres of excellence for processing application specific satellite data
  - *form an integral component of EUMETSAT's distributed application ground segment*
  - *located at National Meteorological Services in Member States*
  - *use expertise of the EUMETSAT community*
  - *use geostationary and polar orbiting satellite data*
  - *generate since few years new products and services for the meteorological and climate user communities*
  - ***Already provide a relevant contribution to GMES and GCOS***

The SAF on Land Surface Analysis is well placed within the GMES Project GEOLAND and involved in the Land Fast Track Service preparation

Support Information

SAF Network Web Area

More Information

Find more information about the SAF Network and keep updated on the Web:

www.eumetsat.int/saf

The SAF Network

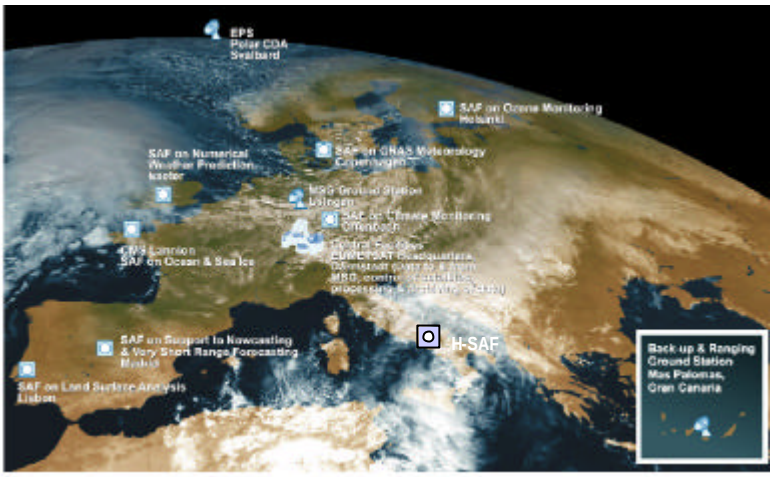

OVERVIEW OF THE LSA SAF DEVELOPMENT & INITIAL OPERATIONS PHASES

Carlos daCamara

ICAT/Faculdade de Ciências da Universidade de Lisboa, Lisboa, Portugal

ABSTRACT

The goal of this communication is to provide an overview of the main achievements of the Satellite Application Facility on Land Surface Analysis (LSA SAF) during its development phase, as well as presenting an account of applications of LSA SAF products already been carried out by the user community. The LSA SAF has initiated its development phase in September 1999 and its main purpose is to develop techniques to retrieve products related with land, land-atmosphere interactions and biospheric applications, using satellite information, namely from Meteosat Second Generation and the forthcoming MetOp. The LSA SAF begun its pre-operational phase in January 2005, and now maintains an operational system fully centralized at the Portuguese Institute of Meteorology (IM). The LSA SAF is currently able to operationally generate, archive, and disseminate a set of pre-operational products; Surface Albedo, Land Surface Temperature, Snow Cover, and Downwelling Surface Short- and Long-wave Fluxes. Although the Numerical Weather Prediction community has been identified as having the greatest potential to fully exploit the LSA SAF products, these also provide relevant information to a wide range of applications, such as agriculture and forestry applications, or the mapping of surface components of the hydrological cycle.

THE LSA SAF LONG-WAVE RADIATION PRODUCTS

I.F. Trigo[1], F. Olesen[2], E. Gajewska[2], I. Monteiro[1], and C. C. DaCamara[3]

[1]Instituto de Meteorologia, Lisboa, Portugal
[2]Forschungszentrum Karlsruhe, IMK, Karlsruhe, Germany
[3]Centro de Geofísica da Universidade de Lisboa, IDL, Lisboa, Portugal

ABSTRACT

The Land Surface Analysis (LSA) Satellite Application Facility (SAF) system, currently operational at Instituto de Meteorologia (IM), Portugal, generates and disseminates on an operational basis the parameters involved in the longwave radiation budget at the surface, i.e, land surface temperature (LST), infra-red (IR) emissivity (EM), and down-welling long-wave surface flux (DSLF). The longwave radiation products are available for the European Continent since February 2005, and for the whole Meteosat disk since July 2005.

The LST retrieval is based on a generalised split-window algorithm, using radiances of Meteosat-8/SEVIRI channels 10.8 μm and 12.0 μm, and respective surface emissivities. The LST algorithm is applied to Meteosat-8 cloud free pixels, according to the cloud mask product of the Nowcasting (NWC) SAF algorithm.

Spectral and broad-band EM are estimated using the so-called vegetation cover method (VCM), which combines retrieved fields of the Fraction of Vegetation Cover (FVC), a land cover database, and EM laboratory measurements. This methodology has been developed for the currently retrieved EM maps (IR10.8 and IR 12.0), as well as for the remaining IR relevant channels (IR3.9 and IR8.7), and for a broadband EM (3-14 μm), e.g., necessary for the estimation of longwave surface fluxes in NWP models.

DSLF can only be indirectly inferred from remotely sensed data. In the LSA SAF approach, DSLF uses two bulk parameterization schemes valid for clear sky and cloudy conditions, respectively. DSLF retrievals benefit from the signature of clouds and different cloud types on IR and VIS channels, complemented with information on atmosphere water content and temperature profiles available from NWP fields.

Product validation includes comparison with in-situ measurements and inter-comparison with similar parameters, retrieved from other satellites. Due to the scarcity of LST ground measurements within the Meteosat disk, the LSA SAF Team has set a permanent station in Evora, Southern Portugal, in an area homogeneous at the SEVIRI spatial scale.

1. INTRODUCTION

The Satellite Application Facility for Land Surface Analysis (Land SAF) has been processing and archiving Land Surface Temperature (LST) and Down-welling Longwave Surface Fluxes (DSLF), on a routine basis, since the kick-off of its Initial Operational Phase (IOP) in January 2005. Currently, the Land SAF LST (DSLF) is derived from SEVIRI/Meteosat data, with a 15 (30) min frequency. The regular archiving of the two products, for a window within Meteosat-8 disk covering most of Europe, has started on the 1st of February 2005, while the processing of the remaining land pixels within the Meteosat disk began in July 2005. The processing of Land Surface Emissivity (EM), needed for LST retrievals, has also begun in February 2005. Since EM is an internal product, it is not distributed regularly.

In order to guarantee the reliability of products provided by LSA-SAF, there is a need to carry out the validation of its products. Apart from comparisons with data obtained from other satellites, the LSA SAF Team has been monitoring the retrieved products against in-situ measurements: Evora (Southern Portugal) for LST, and Carpentras and Roissy (France) for DSLF.

2. LAND SURFACE TEMPERATURE

2.1. LST Algorithm

The Land SAF LST is estimated using a Generalized Split Window (GSW) algorithm. The formulation used by the LSA SAF system was first proposed by Wan and Dozier (1996) to derive LST from AVHRR and MODIS, being later adapted to SEVIRI data (Madeira, 2002). Surface temperature is estimated as a linear function of clear-sky, top of the atmosphere (TOA) brightness temperatures for the split-window channels 10.8μm and 12.0μm (Tb10.8 and Tb12.0, respectively):

$$LST = (A_1 + A_2 \frac{1-e}{e} + A_3 \frac{\Delta e}{e^2}) \frac{T_{10.8} + T_{12.0}}{2} + (B_1 + B_2 \frac{1-e}{e} + B_3 \frac{\Delta e}{e^2}) \frac{T_{10.8} - T_{12.0}}{2} + C \quad (1)$$

where the regression coefficients depend explicitly on the mean surface emissivity for the two channels (ε) and on their difference ($\Delta\varepsilon = \varepsilon 10.8 - \varepsilon 12.0$). The parameters A1, A2, A3, B1, B2, B3, and C, have been empirically estimated for classes of near surface air temperature (2m-temperature), total column water vapour, and satellite viewing angles. Emissivity depends on land cover types and fraction of vegetation (Peres and Dacamara, 2005). Further details on the LSA SAF LST algorithm may be found in the respective Product User Manual (SAF_LAND_IM_PUM_LST_1.2.pdf, available at the LSA SAF web site http://landsaf.meteo.pt/).

The LSA SAF LST product is currently being retrieved and archived operationally, for all land pixels within Meteosat-8 disk, corresponding to viewing angles (VA) lower than 57.5°, since retrieval errors increase significantly for long optical paths. LST estimations use a cloud mask obtained from the NWC SAF software, total column water vapour forecasts provided by the European Centre for Medium-range Weather (ECMWF) forecasts. The product, available via EUMETCast in near real time, or off-line via the LSA SAF website, is then generated pixel-by-pixel, with a 15-min frequency, for the four geographical areas covering Europe, Northern and Southern Africa, and South America, respectively.

2.2. LST Validation

LSA SAF LST is regularly compared against similar MODIS products. Below we show a summary of such intercomparsion exercises, which show the relevance of the instrument viewing angle to the retrieved parameter. Figure 1 presents the daytime MODIS LST product, the corresponding LSA SAF LST field, and the difference between the two. Overall, MODIS LST presents colder values than the corresponding LSA SAF LST. The highest discrepancies, of the order of –3K to –5K, are generally observed during daytime, while night-time discrepancies are generally around –2K to –3K (not shown).

(a) LST_{MODIS} (Daytime)

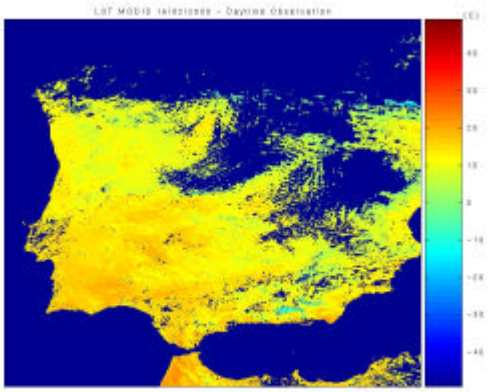

(b) $LST_{Meteosat}$ (Daytime)

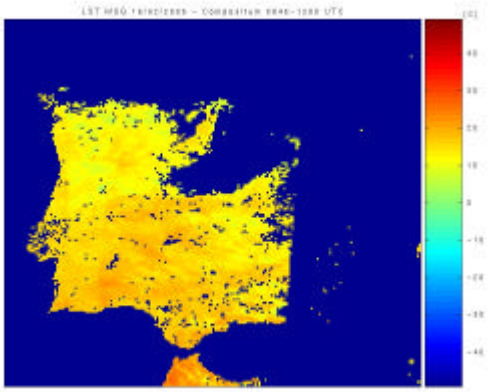

(c) LST_{MODIS} - $LST_{Meteosat}$

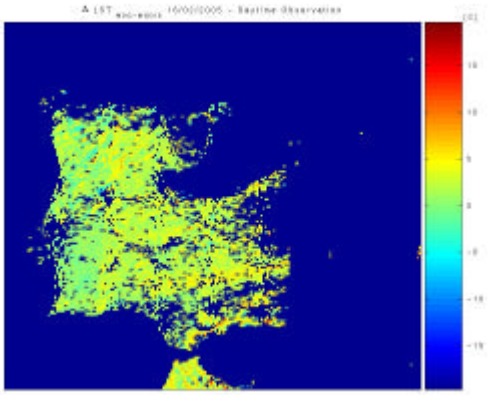

Figure 1: LST (°C) provided for the 16th February 2005 by (a) MODIS, (b) LSA SAF system (Meteosat-8), and (c) the respective difference (MODIS minus Meteosat-8), for the daytime MODIS passage (~11UTC).

MODIS LST values are obtained from a wide range of viewing perspectives, in contrast with the fixed view of geostationary satellites. Positive (negative) MODIS VA indicate the sensor observes the surface from the west (east). The mean differences obtained for daytime LST (red dots in Figure 2) show a very clear dependency on MODIS VA. The discrepancies tend to be higher (Meteosat 6-to-7K warmer than MODIS) for positive VA, while smaller differences (Meteosat ~3 K warmer than MODIS) for VA within the –50° to –35° range. Taking into consideration that the daytime LST (11 UTC) corresponds to local morning over Iberia, the higher (lower) differences occur when MODIS is most likely to observe a higher fraction of shadow (sun-lit) surfaces. Moreover, the VA dependency of daytime LST tends to be more pronounced for the July period, when the temperature contrasts between shadows and illuminated surfaces are higher.

Accordingly, the impact of different MODIS VA on night-time LST (green dots in Figure 2) is small; the slightly higher mean differences for the higher VA classes (above +/- 50°) are most likely associated with the larger uncertainties of the LST algorithm for high optical paths.

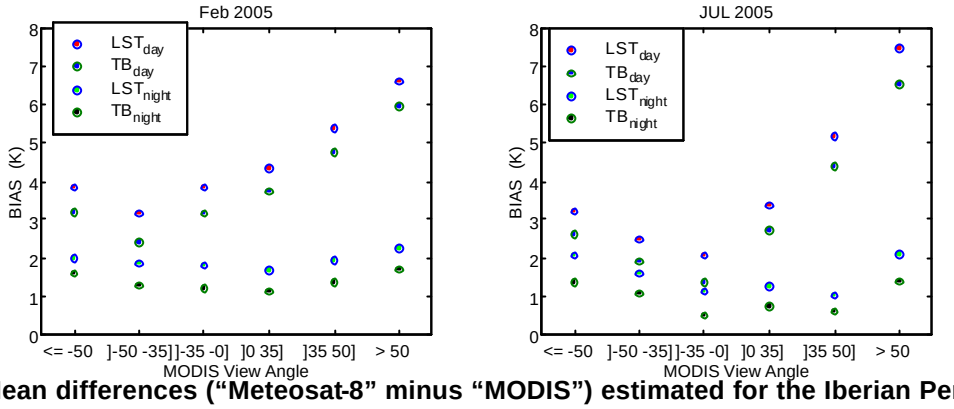

Figure 2: Mean differences ("Meteosat-8" minus "MODIS") estimated for the Iberian Peninsula, for daytime LST (red dots) and surface brightness temperatures (blue dots), and for night-time LST (green dots) and surface brightness temperature (black dots), for the 14-19 Feb (left panel) and 1-7 Jul 2005 (right panel) periods. The values are estimated for the viewing angle (VA) classes shown in the x-axis.

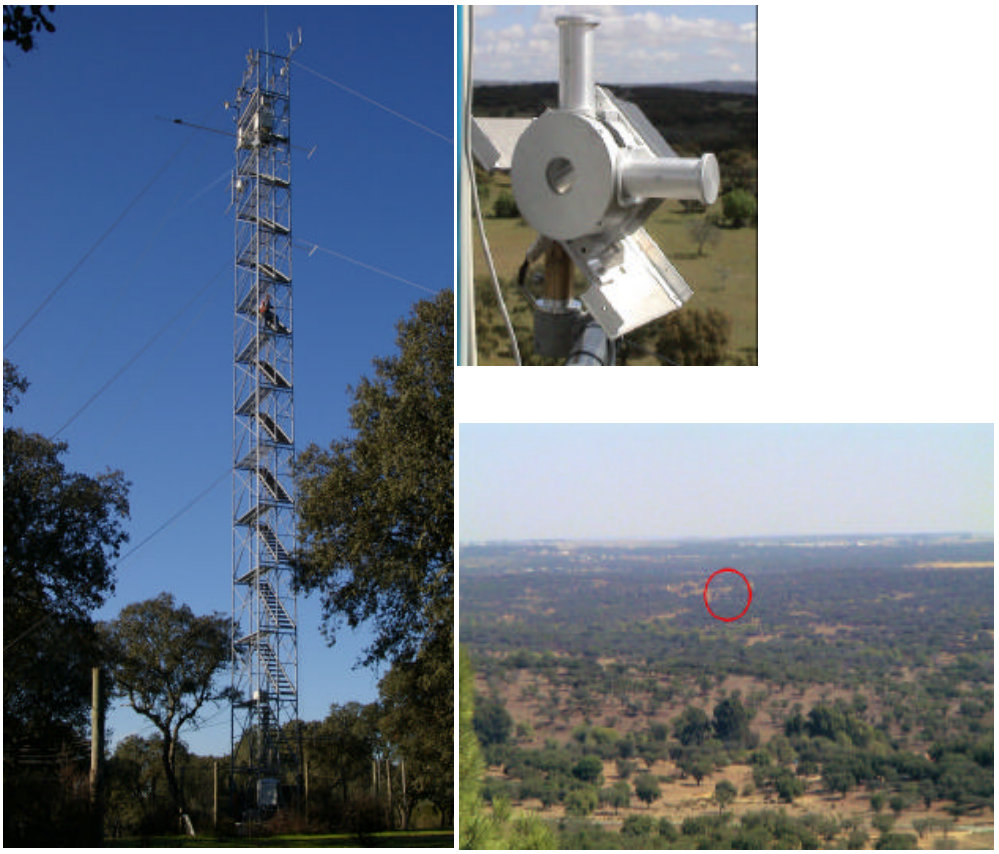

Figure 3: The station in Mitra, Evora (Southern Portugal). Left: the tower (28 m); Top right: the self-calibrating IR radiometer with two blackbody tubes; Bottom right: Panorama view at the station in Mitra, with the tower in the centre of the image.

Intercomparison with other satellite parameters may provide useful insights on the behaviour of the retrieved variables. However, none of those retrievals may be used as an absolute reference in validation, as is the case of ground-truth measurements. The Evora station (Figure 3), currently

used for LST validation, is located in a fairly homogeneous area, allowing for in-situ measurements representative of the satellite pixel. The choice of the location followed a careful selection criterion, which took into account the spatial standard deviation of LST in 20 km x 20 km areas (Dash et al., 2004). Further field investigations of the potential (low standard deviation) sites ascertained the final location, taking into account aspects, such as: (i) the vegetation type is static over years; (ii) vegetation has a smooth annual cycle without sudden changes due to agriculture; (iii) few cloud cover during the year compared to other European regions; (iv) the location assures a viewing angle of the MSG representative for the whole disk.

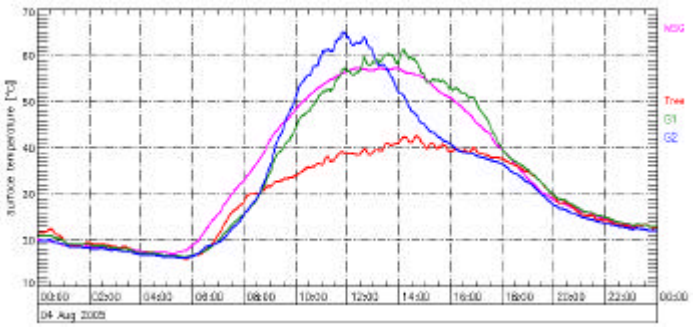

Figure 4: Comparison of LST (magenta) from MSG with measurements from the station for 04. Aug. 2005, taken for: the tree top (red); grass without shadow (G1, green); grass spot, sunlit in the morning and under shadow in the afternoon (G2, blue).

In order to provide representative measurements for the ground truth station, the radiometer was adjusted to point to a tree crown and twice to the grass. Concerning the vicinity of the trees, the grass is partly in shadow during the day, thus it is only partly representative for the whole area. The first comparison results reveal the good agreement for the nighttime. During the daytime, there are big discrepancies between bare-soil and top of canopy in-situ measurements, which make the comparison with LST harder to interpret. In general, the retrieved LST seems to be within the ranges of ground-truth measurements (Figure 4).

3. LAND SURFACE EMISSIVITY

The EM algorithm is based on the so-called vegetation cover method (VCM) (Caselles and Sobrino, 1989) and accordingly EM of each pixel, for channel *c*, e_c, is considered as the result of vegetation, $e_{c,v}$ and bare-ground $e_{c,g}$ portions (Figure 5). Effects of direct, $e_{c,d}$, and internally multi-reflected, de_c, radiances should both be taken into account for each pixel:

$$e_c = e_{c,d} + de_c \quad (2)$$

where:

$$e_{c,d} = e_{c,v}\, FVC + e_{c,g}\, (1-FVC) \quad (2b)$$

$$de_c = 4 \langle de_c \rangle\, FVC\, (1-FVC) \quad (2c)$$

< > denotes the average of de_c within the land cover class, and *FVC* the fraction of vegetation cover.

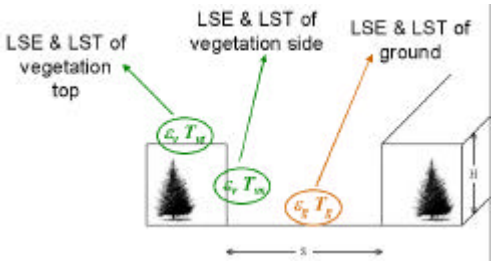

Figure 5: Conceptual model of land surfaces in the VCM.

The LSA SAF EM product relies on Fractional Vegetation Cover (FVC) as the main input, and therefore follows the dissemination rate of the FVC product, i.e., daily and 10-day products are available. The VCM also makes use of a look-up-table developed for spectral and broad-band emissivities, taking into account the spectral response function of each of the SEVIRI channels considered, and laboratory reflectance spectra of different types of surface objects such as vegetation, water, soil, rocks and manmade materials (Peres and DaCamara, 2005). The emissivity laboratory measurements were obtained from Johns Hopkins University (JHU) and Jet Propulsion Laboratory (JPL) spectral libraries included in the Advanced Thermal Emission Reflectance Radiometer (ASTER) library, as well as from the Moderate Resolution Imaging Radiometer–University of California, Santa Barbara (MODIS–UCBS) spectral library. The values of the look-up-table were assigned to surface types based on land cover classification, whereas dynamical information on the proportion of vegetation and exposed surfaces within a pixel is computed based on FVC information.

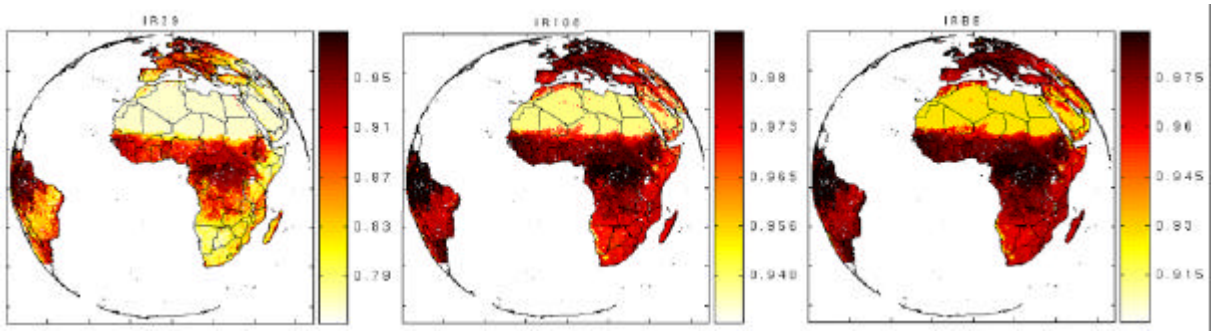

Figure 6: Emissivity examples for IR3.9 (left panel), IR10.8 (central panel) and the broad band (right panel).

4. DOWNWELLING SURFACE LONGWAVE FLUX

4.1. DSLF Algorithm

DSLF (Figure 7) can only be indirectly inferred from remotely sensed data. In the approach used by the LSA SAF, DSLF is estimated using the signature of clouds and cloud types on IR and VIS channels, complemented with information on atmosphere water content and temperature profiles available from NWP fields. It is worth noting the latter, obtained from ECMWF forecasts with ranges between 12h and 24h, include information from atmospheric sounders and other observations, and thus correspond to the best knowledge of atmospheric profiles for each time-slot.

The LSA SAF DSLF algorithm makes use of different bulk parameterization schemes applicable either to clear (Dilley and O'Brien, 1998), or cloudy pixels (Josey et al., 2003), respectively:

$$DSLF_{clear} = 59.38 + 113.7\left(\frac{T_0}{273.16}\right)^6 + 96.96\sqrt{\frac{w}{25}} \quad (3a)$$

$$DSLF_{cloudy} = s\left(T_0 + 10.77N^2 + 2.34N - 18.44 + 0.84(D + 4.01)\right)^4 \quad (3b)$$

The pre-requisites for the DSLF algorithm include 2m temperature (T_0), and 2m dew point depression (D), provided by ECMWF forecasts; cloud information - Cloud Mask, and Effective Cloudiness (N), provided by NWC SAF software, processed at IM; and total precipitable water (w), obtained from ECMWF forecasts. An automatic Quality Control (QC) is performed on DSLF data and the quality information is provided on a pixel basis. The DSLF QC contains general information about input data quality and information about DSLF confidence level.

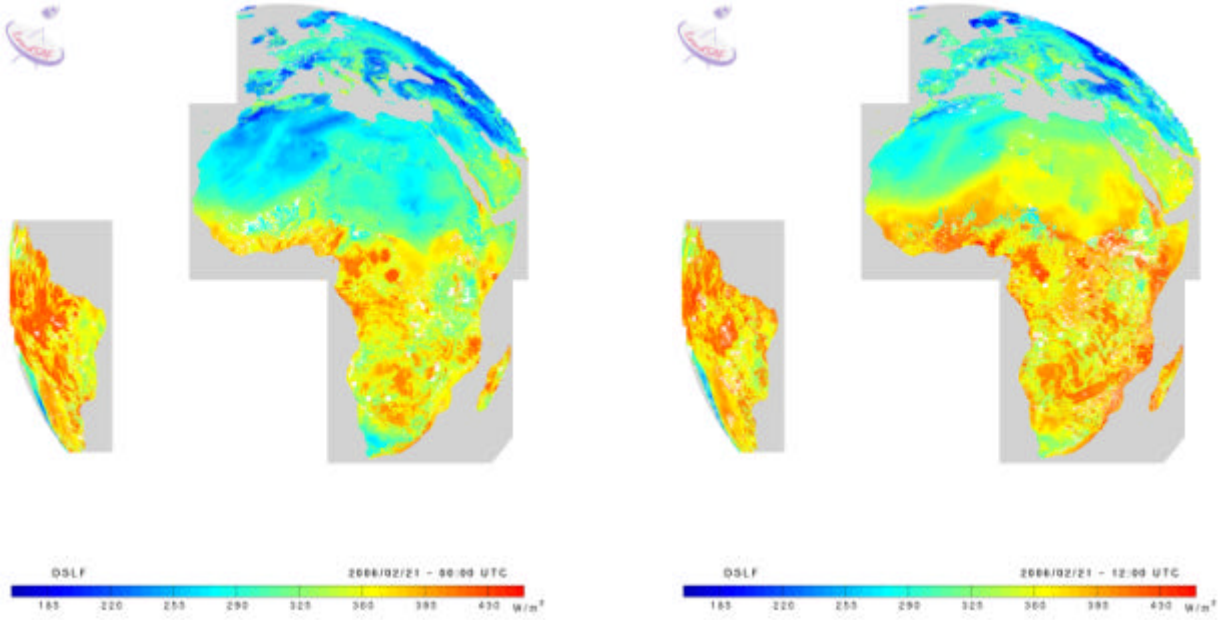

Figure 7: Full disk image of Down-welling Surface Long-wave Fluxes estimated for Feb 19 2006 at 12 UTC.

4.2. DSLF Validation

The validation of DSLF has been focused on the intercomparison of LSA SAF retrieved values with in-situ measurements taken at Carpentras and Roissy (France). The results shown here, corresponding to nearly one-year validation period, generally indicate good agreement between estimated and observed values. However, the clear-sky algorithm tends to underestimate DSLF (green dots in Figure 8). Similar behaviour is also observed for the partially cloudy pixels (blue dots in Figure 8), while fully cloud pixels exhibit the lowest dispersion around the 1:1 line. The root mean square errors, estimated on a monthly basis, generally fall within the 20-30 Wm^{-2} range. Again, the highest mean discrepancies are obtained for clear and partially cloud cases. The largest values are found for cases where the pixel is classified as “partially cloudy”, which also have the greatest uncertainties in cloud information.

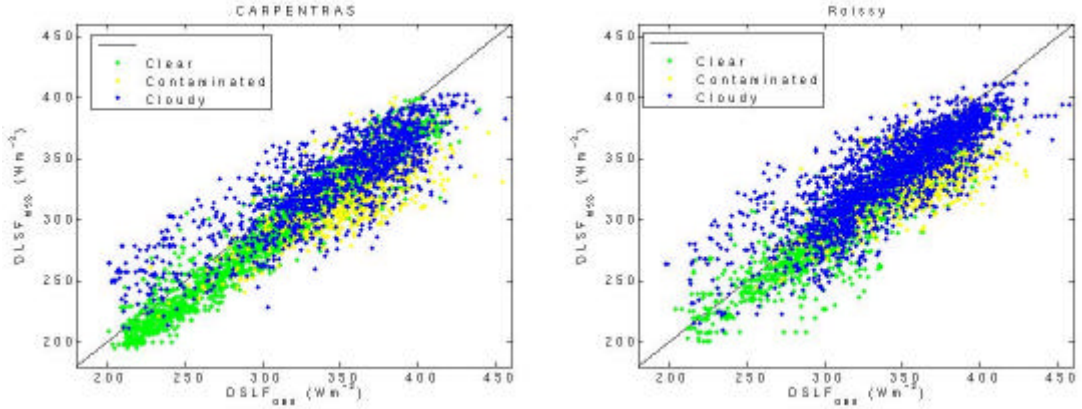

Figure 8: Scatterplots of Land SAF DSLF (y-axis) versus in-situ measurements (x-axis), for Carpentras (left) and Roissy (right), for the January-October 2005 period. The dots are coloured according to the following correspondence: green - clear-sky pixel; yellow – partially cloudy; and blue – cloudy pixel.

The next step in the validation of DSLF will be extending the comparison with ground-truth values to further sites, particularly in Africa. The LSA SAF Team will make use of data acquired during field campaigns lead by other projects, when the data are considered reliable and made available to external partners. As an example it is foreseen to use surface flux measurements to be obtained by the AMMA project over Africa.

5. CONCLUSIONS AND FUTURE WORK

The LSA SAF is part of the SAF Network, i.e., specialised development and processing centres, which constitute EUMETSAT distributed Applications Ground Segment, along with the Central Facility in Darmstadt. The main purpose of the SAF dedicated to Land Surface Analysis is to take full advantage of remotely sensed data, particularly those available from EUMETSAT sensors, to describe/derive land surface properties/variables. The LSA SAF has started its 5-year development phase in September 1999, and its initial operations in January 2005. While algorithm development, maintenance and validation is distributed among all members of the Consortium, the LSA SAF operational system is fully centralised at IM. The latter is now generating and archiving three long-wave radiation products – Land Surface Temperature (LST), spectral and broad-band emissivity (EM), and downwelling surface longwave flux (DSLF). EM is considered an internal product (used for the estimation of LST), and thus is not generally available to users, unless there is a specific request.

The LSA SAF products in general, and the long-wave radiation parameters in particular, are continuously monitored against similar parameters retrieved from other satellites, and ground-truth measurements, whenever possible. Within this line LST is compared against MODIS retrievals, and will soon begin to be compared regularly with AATSR LST. The goal of such exercises is to identify all the factors that might influence algorithm performance, including different emissivity maps in use, cloud masking, and viewing angles. Ground-truth data should provide an independent and reliable reference, although up-scaling issues may be difficult to deal with. To minimise such problems, the Evora site (Southern Portugal), set up by the LSA SAF team as a ground-truth site for LST, is located in a fairly homogeneous region, with stable vegetation cover, and smooth inter-annual cycle.

Preliminary results show that LSA SAF LST follows well the MODIS product, and in-situ measurements taken in Evora. Daytime discrepancies tend to be higher than those observed during the night period, in both cases. The comparison with MODIS shows strong dependency with satellite viewing angle (VA) during the day, with the most pronounced differences (> 4 K) occurring for positive MODIS VA, typically higher than 35°. In this case, MODIS sensor observes the Iberian Peninsula from the West. Since the observation time corresponds to local morning, the probability of MODIS viewing a higher fraction of shadow surfaces, when compared with the South-east Meteosat observations, is also higher. As expected the influence of MODIS VA on night-time discrepancies is negligible. These results strongly suggest that LST fields retrieved from remote sensing platforms are highly dependent on the viewing angle for daytime time-slots, unless a correction for the angular effects is provided.

Land surface emissivity is an important quantity for the estimation of LST, but also for a correct evaluation of the surface energy budget. The current EM algorithm combines information on the fraction of vegetation cover with land cover classification and emissivity look-up-tables, built up with existing spectral emissivity libraries. An intercomparsion with other EM databases, including that used for MODIS LST retrievals is ongoing.

The complete assessment of the estimated downward longwave fluxes at the surface (DSLF) clearly requires further validation sites. Those used so far for comparison with in-situ data, located in France, indicate that about 40% of the cases present relative errors lower than 5%, and 40% present errors between 5 and 10%. Collaboration with other projects, such as AMMA, will provide further validation data in the near future.

The next phase of the LSA SAF, the Continuous Development and Operations Phase CDOP, is envisaged to last 5 years between March 2007 and February 2012. During the CDOP, the LSA SAF consortium will pursue two main goals:

1. The consolidation of operational activities (i.e., the generation, dissemination, and archiving of land surface related products), including the monitoring of the LSA SAF operational system, the helpdesk service, and general user support (updated website, workshops).
2. Continue Research and Development (R&D) activities necessary for
    - Validation of LSA SAF products;
    - Improvement of existing products following new user requirements and/or the adaptation to new sensors, including the preparation for post-MSG (MTG), and post-EPS data;
    - Development of new land surface related products, to be operational during the CDOP;
    - Upgrading of the LSA SAF system, following the demands of new operational products and/or sensors to be processed.

The LSA SAF products will continue to be accessible via EUMETCast, or ftp (http://landsaf.meteo.pt). The LSA SAF addresses a wide community, ranging from surface processes modelling – e.g., NWP, seasonal forecasting, climate models – to agriculture and forestry applications – e.g., fire hazards, food production – and hydrology. Such community greatly benefits from products generated from a reliable observation system designed to ensure long-term operations, such as the EUMETSAT geostationary and future polar satellites.

6. BIBLIOGRAPHIC REFERENCES

CASELLES, V., and SOBRINO J. A., (1989) Determinating of frosts in orange groves from NOAA-9 AVHHR data. Remote Sens. Environ., **29**, pp 135-146

DASH, P., F.-S. OLESEN, and A. J. PRATA (2004): Optimal Land Surface Temperature validation site in Europe for MSG. Proceedings of EUMETSAT Meteorological Satellite Conference, Prague, 31May-4June 2004, 248-264.

DILLEY, A.C. and D.M. O´BRIEN, (1998) Estimating downward clear sky long-wave irradiance at the surface from screen temperature and precipitable water, Q. J. R. Meteorol. Soc., 124: 1391-1401.

JOSEY, S.A., R. W. PASCAL, P. K. TAYLOR, and M. J. YELLAND, (2003) A new formula for determining the atmospheric longwave flux at the ocean surface at mid-high latitudes. J. Geophys. Res., 108: doi: 10.1029/2002JC001418.

MADEIRA, C., (2002) Generalised split-window algorithm for retrieving land-surface temperature from MSG/SEVIRI data. SAF on Land Surface Analysis Training Workshop, Lisbon, Portugal, July 8-10.

PERES, L.F. and DACAMARA, C.C., (2005) Emissivity Maps to Retrieve Land-Surface Temperature From MSG/SEVIRI. IEEE Trans. Geosci, Remote Sens., **43**, pp 1834-1844

WAN Z. and DOZIER, J., (1996) A generalized split-window algorithm for retrieving land surface temperature from space. IEEE Trans. Geosci, Remote Sens., **34**, pp 892-905

THE LAND-SAF SURFACE ALBEDO AND DOWNWELLING SHORTWAVE RADIATION FLUX PRODUCTS

B. Geiger[1,2], D. Carrer[1], L. Franchistéguy[1], D. Lajas[1,3], C. Meurey[1], and J.-L. Roujean[1]

[1] Météo-France/CNRM, 42 avenue Gaspard Coriolis, 31057 Toulouse Cedex, France
[2] Instituto de Ciência Aplicada e Tecnologia, Campo Grande, 1749-016 Lisboa, Portugal
[3] Faculdade de Ciências da Universidade de Lisboa, 1749-016 Lisboa, Portugal

ABSTRACT

Within the Satellite Application Facility for Land Surface Analysis we developed algorithms for the derivation of land surface albedo and down-welling short-wave radiation flux from Meteosat Second Generation data. The corresponding processing chains were implemented in the operational system and the products covering Europe, Africa, and a part of South America are now generated and provided to the user community in near real time.

The albedo and down-welling radiation products are both based on the visible channels of the SEVIRI imaging instrument. Albedo maps are generated once a day by using the most recent cloud-free observations available. The algorithm consists in the application of a bi-directional model to the atmospherically corrected reflectance factor observations. Using the previously available estimate as a priori information in a recursive scheme makes it possible to achieve at the same time a high temporal resolution and a good spatial coverage of the albedo product.

Instantaneous estimates of the short-wave radiation flux are currently calculated with a temporal frequency of thirty minutes. Depending on the presence of clouds different methodologies are used to retrieve this quantity. For cloudy sky the signal measured at the top of the atmosphere is used as input information for a physical model of the cloud-atmosphere-surface system in order to retrieve the flux estimate. For clear sky situations a parameterisation as a function of geometry and atmospheric constituents is applied.

The consistency of the albedo product has been checked by comparing the results with equivalent products derived from other instruments. The down-welling short-wave radiation flux product on the other hand has been validated with in-situ measurements acquired at several ground stations.

1. INTRODUCTION

The Satellite Application Facility for Land Surface Analysis hosted by the Portuguese Meteorological Institute in Lisbon generates and distributes value added satellite products for numerical weather prediction and environmental applications in near-real time. Since the beginning of the Initial Operational Phase in 2005 Meteosat Second Generation data are routinely processed by the Land-SAF operational system.

Within the project consortium Météo-France is responsible for the land surface albedo and down-welling surface short-wave radiation flux (DSSF) products which are both derived from the 0.6µm, 0.8µm, and 1.6µm channels of the SEVIRI instrument. These products are currently classified as "pre-operational" which signifies according to the relevant EUMETSAT terminology that they are "able to satisfy the majority of applicable requirements" and have been considered "suitable for early distribution to SAF users with documented limitations".

In the Land-SAF system four continental windows (Europe, North of Africa, South of Africa, and South America) are separately processed and distributed in the native MSG/SEVIRI projection. The product files are disseminated with a specified timeliness of three hours via the Land-SAF website (http://landsaf.meteo.pt/) and by the EUMETSAT broadcast system EUMETCast.

2. SURFACE ALBEDO

The surface albedo quantifies the fraction of incident solar radiation that is reflected by the Earth's surface. It therefore constitutes an important element for characterising the surface energy balance. Since the albedo is "relatively close" to the physical measurements obtained by remote sensing one can expect to retrieve this quantity with a reasonable accuracy.

2.1. Methodology

The retrieval scheme comprises four successive steps: First the measured top-of-atmosphere radiances delivered by the satellite instrument are corrected for atmospheric effects in order to convert them into the corresponding top-of-canopy (TOC) reflectance factor values. The spectral TOC-reflectances then serve as the input quantities for the inversion of a linear model of the bi-directional reflectance distribution function (BRDF) which quantifies the dependence on the illumination and observation geometry. Spectral albedo values in the instrument channels are determined from the angular integrals of the model functions with the retrieved parameter values. Finally, a narrow- to broad-band conversion is performed with a linear regression formula.

Technically the processing chain comprises two distinct modules - one for atmospheric correction and one for model inversion and directional and spectral integration. The atmospheric correction module is applied separately on each image directly after acquisition. The inversion and albedo calculation module, on the other hand, operates on a set of TOC-reflectance images collected during one day. By using the previous inversion result as a priori information in a recursive scheme, a temporal composition of the information over a longer time period can be achieved in order to guarantee the coherence and completeness of the product while still preserving a rather high temporal resolution. Figure 1 (left) shows the resulting effective temporal weight for the observations as a function of the difference with respect to the nominal product time. The physical and mathematical background of the algorithm is explained in the Product User Manual (Land-SAF, 2005) available on the project website. Relevant references are also listed in this document.

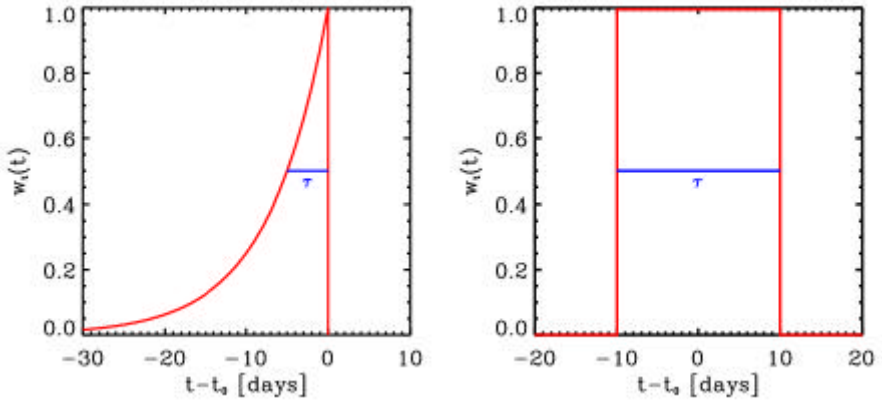

Figure 1: Left: Effective temporal weight function in the recursive composition scheme with a characteristic time scale of t = 5 days. Right: "Classical" composition window envisaged for a variant of the albedo product with different temporal characteristics (cf. Section 5).

2.2. Product Characteristics

The albedo product is generated on a daily basis. It comprises spectral albedo estimates corresponding to the three used SEVIRI channels as well as broad-band albedo estimates for the visible [0.4µm, 0.7µm], near infrared [0.7µm, 4µm], and total short-wave [0.3µm, 4µm] intervals. Full disk example images generated by re-composing the four continental windows are shown in Figure 2. The provided quantities include the directional-hemispherical (or 'black-sky') albedo at local solar noon and, for the spectral and total broad-band estimates, also the bi-hemispherical (or 'white-sky') albedo. The latter is relevant for a completely diffuse sky while the former corresponds to the presence of direct illumination only.

For each of the albedo quantities an uncertainty estimate is calculated by propagating estimates for the non-correlated (random) part of the input data errors through the model inversion (see the Product User Manual for details). The resulting values therefore quantify the contribution to the uncertainty due to random error sources and depend mainly on the number of observations available, the estimated TOC-reflectance errors, and the respective angular configuration. Sources of systematic errors, e.g. instrument calibration, are not taken into account in these uncertainty estimates. An example is depicted in Figure 3. The quality flag also shown in this figure contains information about the land/water mask, the processed regions and potential snow cover.

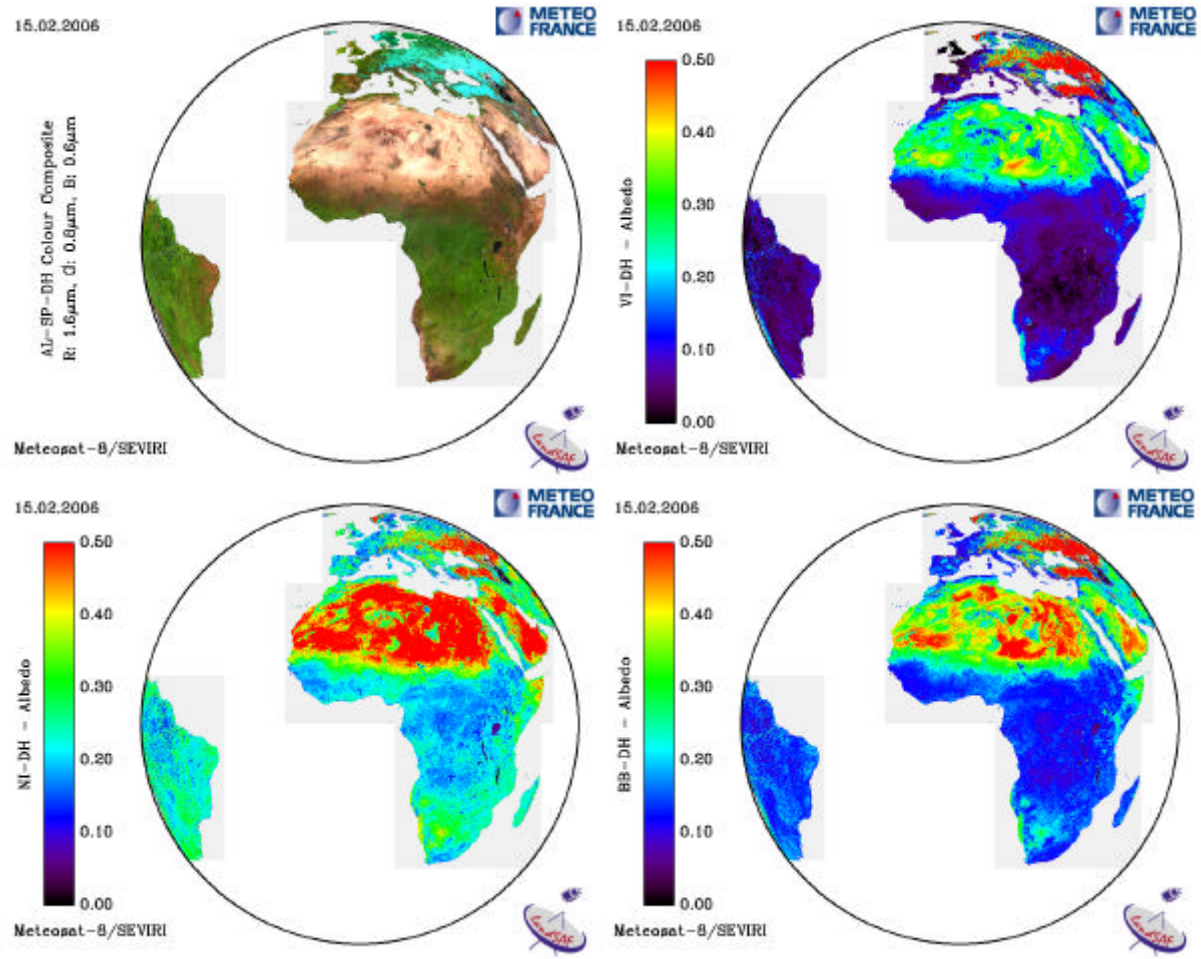

Figure 2: Directional-hemispherical albedo product images for the 15th of February 2006. Top Left: Colour composite of the three spectral albedo estimates. Top Right: Visible broad-band. Bottom Left: Near Infrared broad-band. Bottom Right: Total short-wave broad-band.

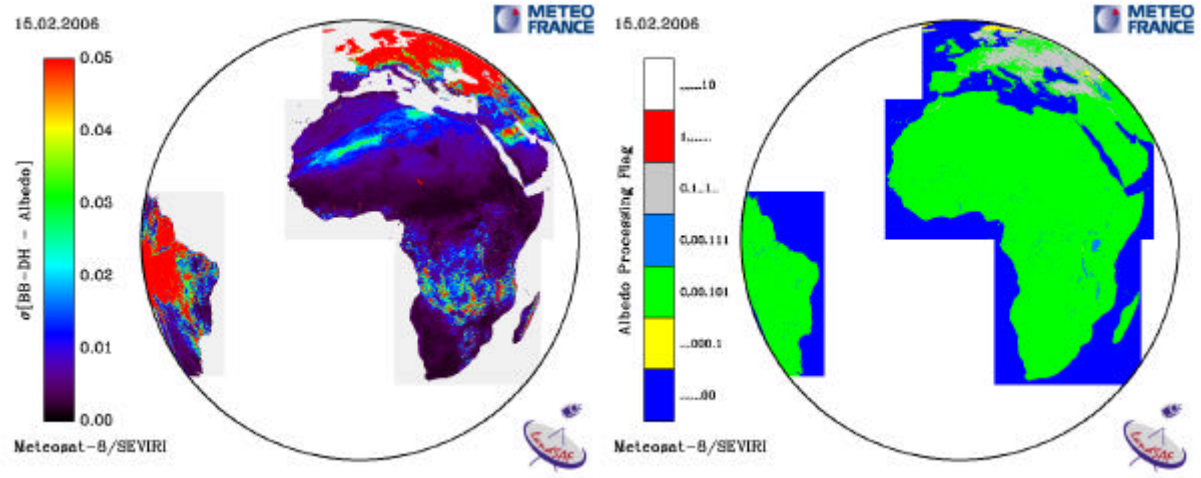

Figure 3: Left: Example for the uncertainty estimates (total broad-band directional-hemispherical). Right: The quality (or processing) flag for the 15th of February 2006. The processed areas appear in green, light blue (continental water), or grey (snow), and unprocessed areas in blue (ocean) and yellow.

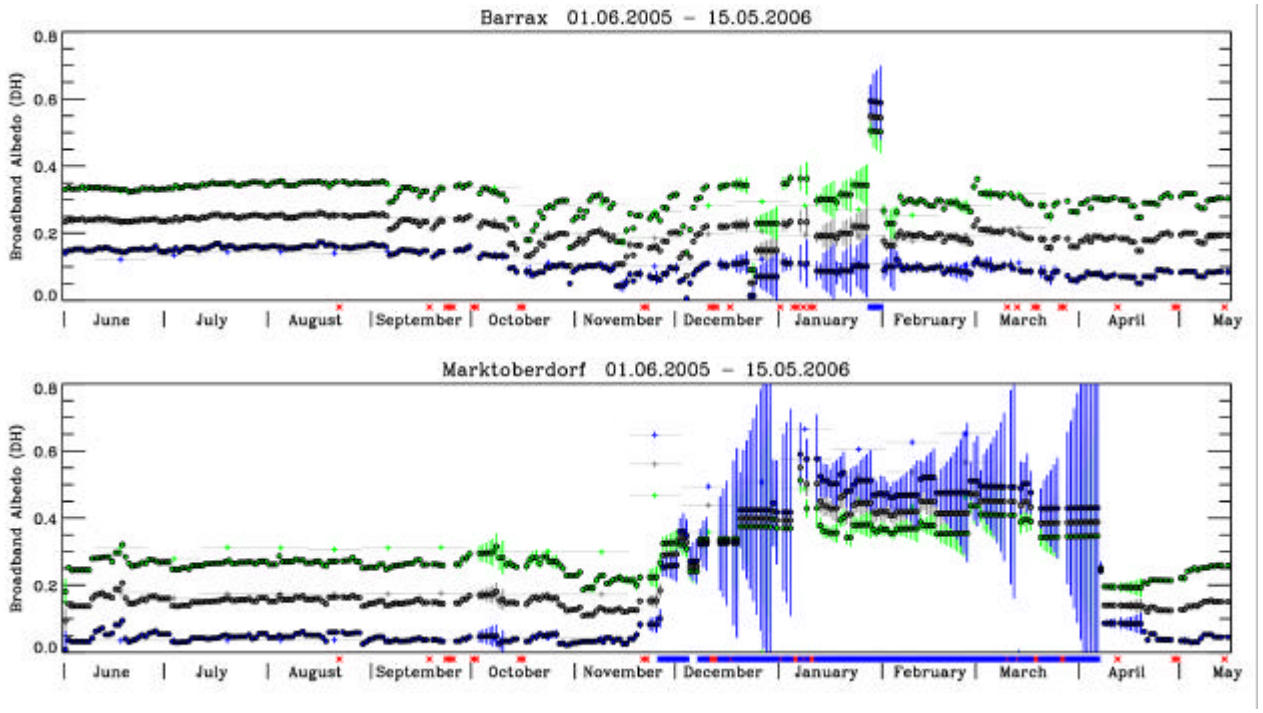

Figure 4: Time series of directional-hemispherical broad-band albedo estimates for image pixels corresponding to the location of Barrax (Albacete, Spain) and Marktoberdorf (Allgäu, Germany). The colours grey, blue, and green, respectively, correspond to the total short-wave range, to the visible, and to the near infrared. The vertical bars indicate the respective uncertainty estimates. (For low values they may be entirely covered by the dot symbol.). A red cross on the time axis indicates that no product file was generated by the operational system for the respective day. The blue star indicates that the pixel was flagged as snow covered. The graphs also include MODIS albedo estimates marked by crosses with horizontal bars indicating the respective temporal composition window.

Finally, Figure 4 shows the resulting time series for two example sites. The largest albedo changes are provoked by snowfall and snowmelt. The seasonal evolution of vegetation and changes of soil humidity also induce temporal variability of the surface albedo. The product time series may still contain high frequency noise caused by uncorrected atmospheric effects (e.g. due to variations of the aerosol concentration on small time scales) or by potential problems in the elimination of observations affected by clouds or cloud shadows. The rapidly increasing uncertainty estimates that can be seen for example at the end of December reflect the lack of information during periods without useful observations due to persistent cloudiness.

2.3. Validation

The albedo product has been (indirectly) validated by comparing it to the respective product derived from observations of the MODIS instrument, which is generally considered as being of good quality and suitable as a reference quantity. We re-projected the higher resolution MODIS product to the MSG/SEVIRI grid within the European continental window. For each original MODIS pixel the “closest” SEVIRI pixel was determined and afterwards the albedo estimates for all MODIS pixels assigned to a given SEVIRI pixel were averaged. The MODIS product is generated with a temporal composition window of 16 days. In order to reproduce the temporal characteristics as closely as possible with the MSG data, the internal TOC-reflectance files provided by the operational system were re-processed to generate daily albedo estimates, which were then averaged over the relevant MODIS period. An example of the resulting MSG and MODIS product images is shown in Figure 5. Visually the two maps compare very well. The dynamic range of the

occurring albedo values is slightly larger for the Land-SAF product. In the time series of Figure 0 the MODIS data points corresponding to the selected sites are also included.

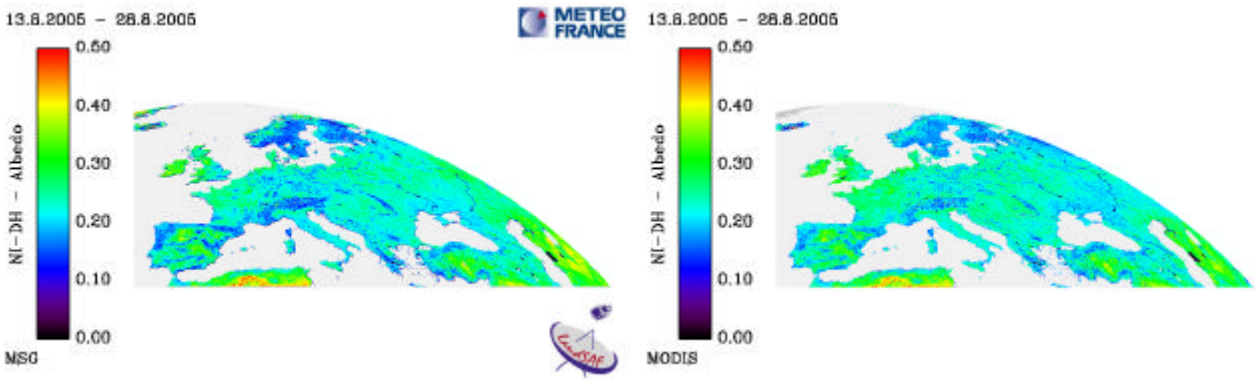

Figure 5: Comparison of directional-hemispherical near infrared broad-band albedo results for the period between the 13th and the 28th of August 2005. Left: Land-SAF albedo. Right: Re-projected MODIS albedo.

Figure 6 depicts scatter plots – or rather probability density plots – for the different broad-band albedo quantities derived from the two instruments. The graphs show that for the selected period there are no systematic differences in the near infrared and total short-wave estimates. For the visible broad-band range, however, the Land-SAF product slightly overestimates the albedo with respect to MODIS.

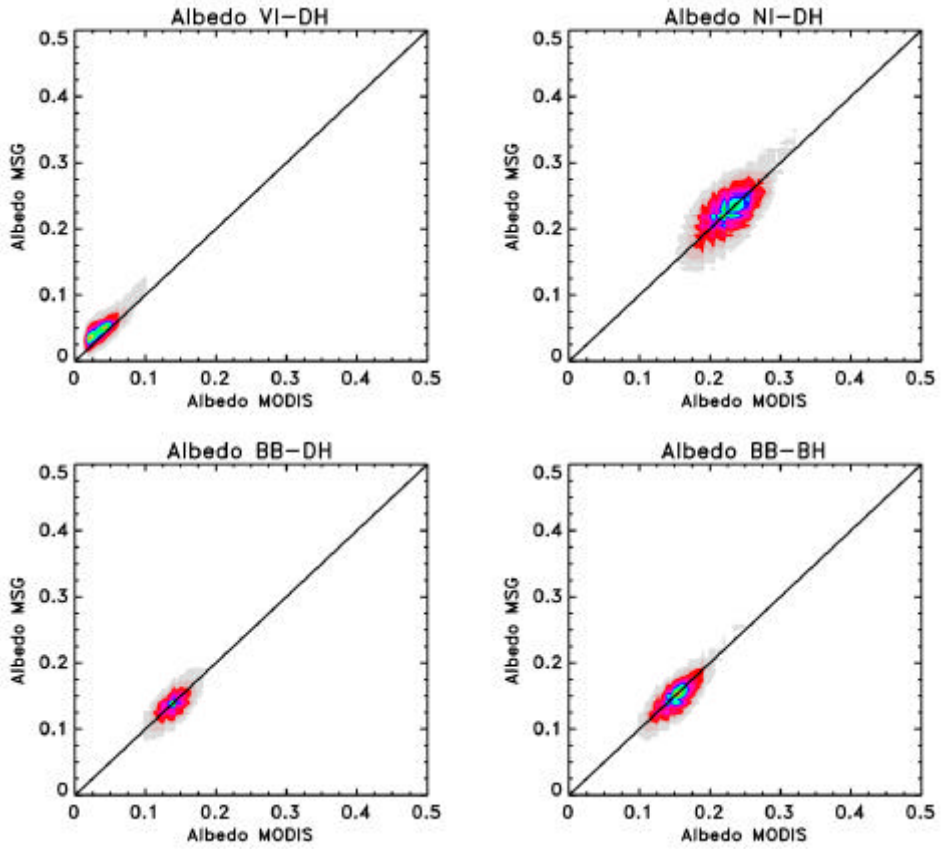

Figure 6: Scatter plots between the Land-SAF and MODIS albedo results for the period between the 13th and the 28th of August 2005. Top Left: Visible directional-hemispherical. Top Right: Near Infrared

directional-hemispherical. Bottom Left: Total short-wave directional-hemispherical. Bottom Right: Total short-wave bi-hemispherical.

For expressing the validation results in a quantitative way we determine the bias – defined as the average of the difference between the two estimates – and the standard deviation of that difference. The temporal evolution of the validation statistics from June 2005 to March 2006 is visualised in Figure 7. The position of the symbols in the graphs indicates the bias, and the length of the bars (from the centre to each end) corresponds to the standard deviation as defined above. The calculation of the statistics was restricted to those pixels for which the Land-SAF uncertainty estimate is below 0.10 and the MODIS quality flag indicates a high confidence.

Until the month of October, the biases between the Land-SAF and MODIS products are negligible for the near infrared and total short-wave ranges and in the order of +0.015 for the visible range. The standard deviation in absolute units ranges between 0.015 for the visible and up to 0.03 for the near-infrared and total short-wave ranges. However, owing to the lower level of the albedo values, the discrepancies in relative units are the largest for the visible broad-band estimates. The results tend to deteriorate during winter, which may be related to the unfavourable observation conditions (clouds, low solar elevation), the smaller number of data points entering the validation statistics, and the different treatment of snow cover in the Land-SAF and MODIS algorithms.

The validation studies will be pursued in more detail by considering the spectral albedo quantities and by investigating the performance as a function of season, geographic position, surface type, snow cover, precipitation, or atmospheric composition.

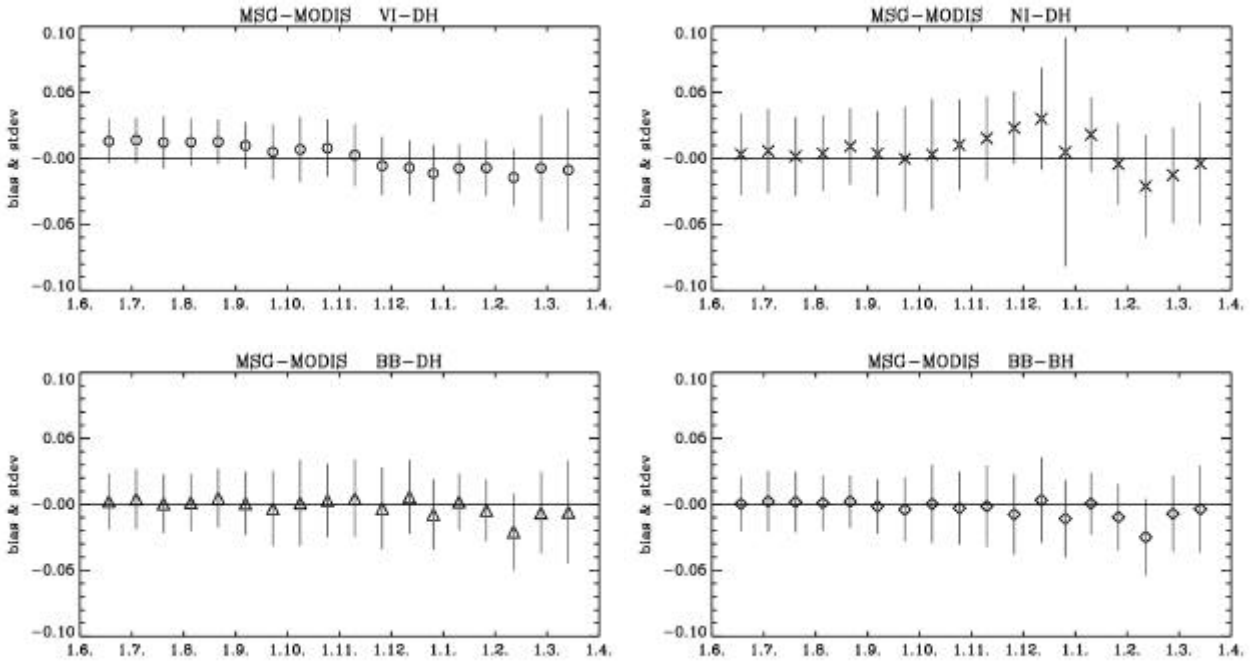

Figure 7: Time series of the albedo validation statistics (in absolute units) from June 2005 to April 2006. Top Left: Visible directional-hemispherical. Top Right: Near Infrared directional-hemispherical. Bottom Left: Total short-wave directional-hemispherical. Bottom Right: Total short-wave bi-hemispherical.

3. DOWNWELLING SURFACE SHORTWAVE RADIATION FLUX

The down-welling surface short-wave radiation flux (DSSF) refers to the radiative energy in the wavelength interval [0.3µm, 4.0µm] reaching the Earth's surface per time and surface unit. It essentially depends on the solar zenith angle, on cloud coverage, and to a lesser extent on atmospheric absorption and surface albedo.

3.1. Methodology

The method for the retrieval of DSSF currently implemented in the Land-SAF system largely follows previous developments achieved at Météo-France in the framework of the SAF on Ocean & Sea-Ice (OSI SAF, 2002). Separate algorithms are applied for clear sky and cloudy sky situations. In the presence of clouds, the down-welling radiation reaching the ground is considerably reduced. The DSSF is strongly anti-correlated with the observable top-of-atmosphere reflectances: The brighter the clouds appear on the satellite images, the more radiation is reflected by them and the less radiation reaches the surface. In this case the top-of-atmosphere albedo is first calculated from the observed directional reflectance values by applying a broad-band conversion and an angular dependence model. The top-of-atmosphere albedo then serves as the most important input information for a simple physical model of the radiation transfer in the cloud-atmosphere-surface system. In the clear sky method the DSSF estimate is directly determined with a parameterisation for the effective transmittance of the atmosphere as a function of the concentration of atmospheric constituents. A more detailed description is given in the Product User Manual (Land-SAF, 2006).

3.2. Product Characteristics

The DSSF estimates are currently calculated at intervals of thirty minutes based on every second slot of MSG/SEVIRI images. The values are derived for the instantaneous acquisition time of each image line. The SEVIRI scans are performed from South to North. At the Northern edge of the image the reference time therefore deviates from the nominal slot time by up to twelve minutes.

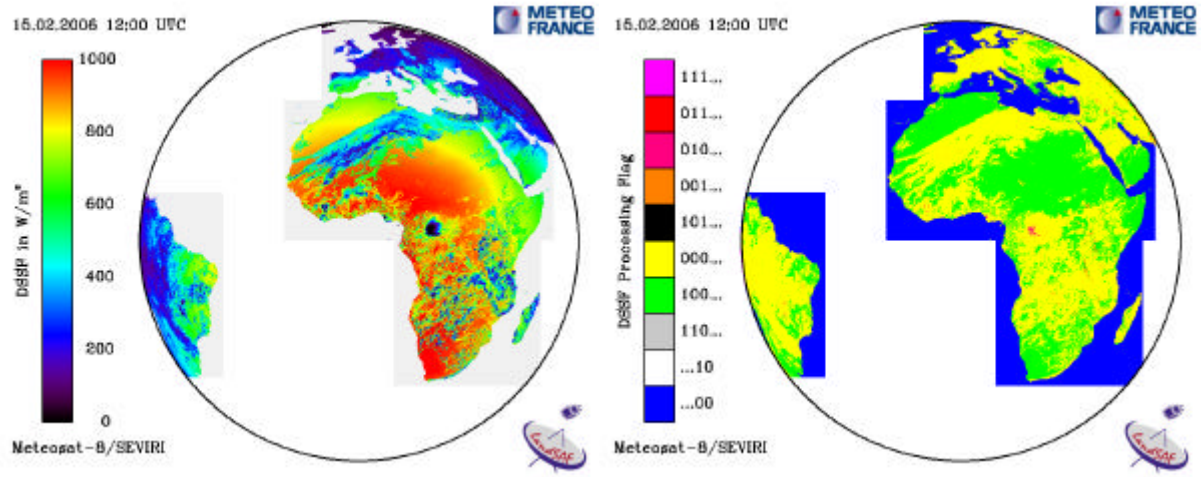

Figure 8: The DSSF estimate (left) and the corresponding quality (or processing) flag information (right) generated for the 15th of February 2006 at 12:00 UTC.

The DSSF product files comprise the physical estimate as well as a quality flag. An example is given in Figure 8. In the visualisation of the quality information the green colour refers to the regions for which the clear sky method was applied, the yellow colour indicates the application of the cloudy sky method, and the blue colour marks the ocean for which no estimates are derived.

The other colours appearing in the legend refer to particular cases which do not occur very frequently. The detailed signification of the bit codes is explained in the Product User Manual.

3.3. Validation

Up to now the validation studies have been based on the Baseline Surface Radiation Network (BSRN) stations of Carpentras (France) and Toravere (Estonia) for which data concomitant with our product time series were already available. In addition we had access to in-situ data from ground measurement stations run by the Land-SAF project in Evora (Portugal) and by Météo-France in Roissy (France).

In general a good agreement between the satellite estimates and the in-situ data is observed when comparing the daily time series. A few examples are shown in Figure 9. In the unfavourable case depicted for Roissy with a rather large dispersion, the discrepancies cannot entirely be attributed to deficiencies of the retrieval method. The example also illustrates the limitation of the validation approach when the conditions are highly variable in space and time. At least part of the dispersion is a consequence of comparing a local measurement with an estimate for a rather extended image pixel.

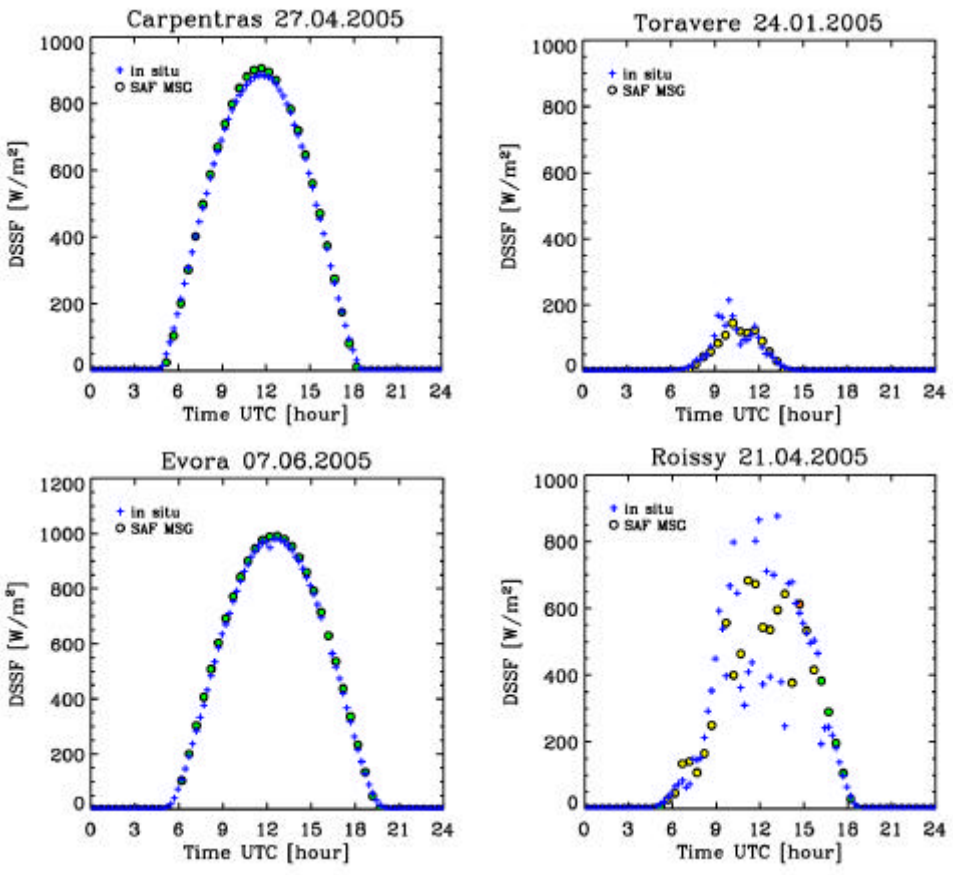

Figure 9: Examples for daily time series of DSSF estimates and in-situ measurements at the ground validation stations. The colour code of the dots is the same as for the quality flag in the previous figure.

Figure 10 depicts scatter plots of the Land-SAF estimates against the in-situ measurements for the whole available validation period. The top left plot includes all data points for Carpentras for which the clear sky method was applied and the top right plot all “cloudy” data points for Roissy. As

expected the dispersion of the distribution is much smaller for the “clear” than for the “cloudy” data points. The biases are relatively small in both cases and there is no significant evidence for a dependence of the bias on the level of the DSSF estimate. A few outliers can be perceived in the scatter plot for clear sky. However, their number is quite small compared to the large amount of data points included in the graph. The outliers may be caused by geo-location uncertainties or by small clouds which obstructed the direct solar radiation but could not be detected on the pixel scale.

The bottom left plot of Figure 10 includes all available data points for the site of Evora. For validation purposes we also calculated daily averages of the Land-SAF DSSF product for the pixels corresponding to the validation sites. This is helpful for comparing the quantitative validation statistics to those of other products which are not available as instantaneous estimates. The daily values are determined by averaging all available (day-time) Land-SAF DSSF estimates for a given day. For comparison only the in-situ measurements corresponding to the product time slots actually used for the determination of the “daily DSSF product” are then also averaged to obtain the corresponding “daily averaged in-situ measurement”. (Note that this prescription is useful only for our validation purposes, but not appropriate for generating a daily averaged DSSF product meant to be distributed and utilised. For this purpose the problems of temporal reference for the average and the treatment of missing data would have to be considered much more carefully.) The resulting data points for Evora are depicted in the bottom right plot of the figure. As expected the dispersion is much smaller than for the instantaneous radiation estimates.

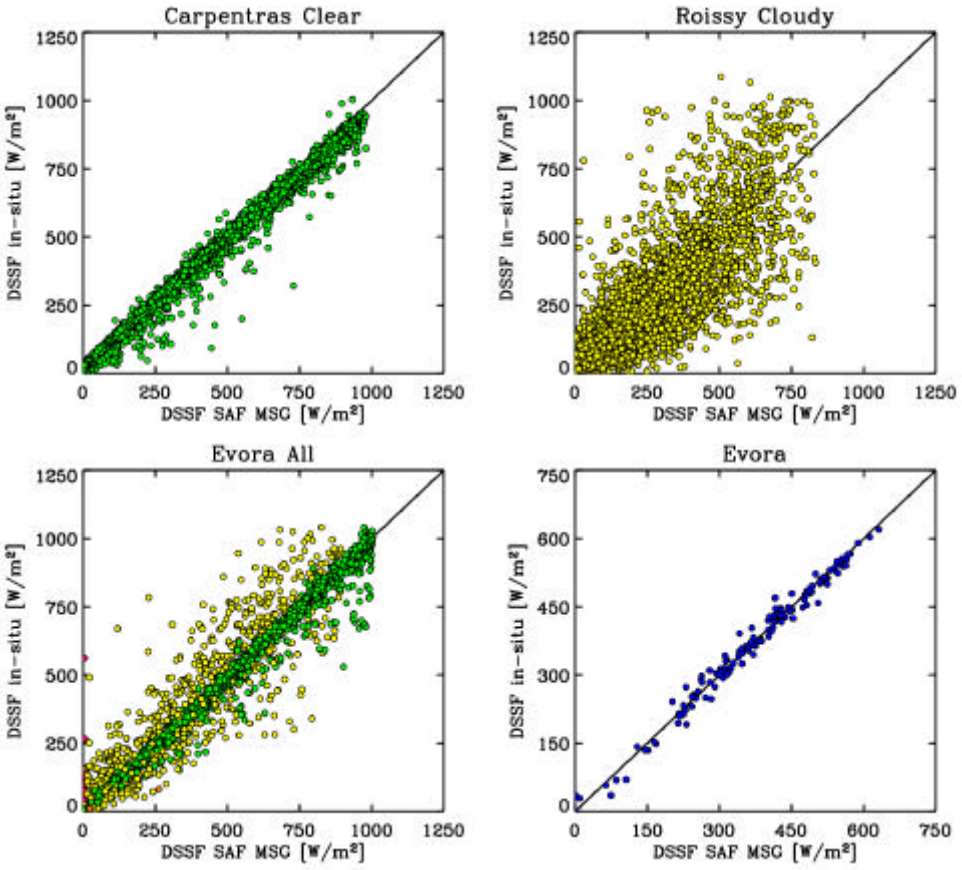

Figure 10: Scatter plots between the satellite estimates and the ground measurements. The colour code of the dots is the same as for the quality flag in the previous figures. The bottom right plot shows the daily averaged estimates as explained in the text. Note that the shown range of values is different in this case.

The temporal evolution of the statistical quantities – bias and standard deviation – for all four stations combined over the whole available validation period is shown in Figure 11. Monthly sub-samples of the validation data points are considered in order to illustrate a possible temporal evolution of the product quality. From the top left to the bottom right the panels show the results for the data points processed with the clear sky method, for the cloudy sky method, for all processed day-time data points combined irrespective of the method applied, and for the daily averaged DSSF values which were calculated for validation purposes only as described above. The top left plot for clear sky also includes the bias values (but not the standard deviation) for morning and afternoon data points separately. Considering the whole validation period and all sites there is a small positive bias in the order of 5 Wm^{-2} for both clear and cloudy sky situations. The standard deviation is in the order of 40 Wm^{-2} for the clear sky and 115 Wm^{-2} for the cloudy sky (instantaneous) estimates while it reduces to 30 Wm^{-2} for the daily averaged values.

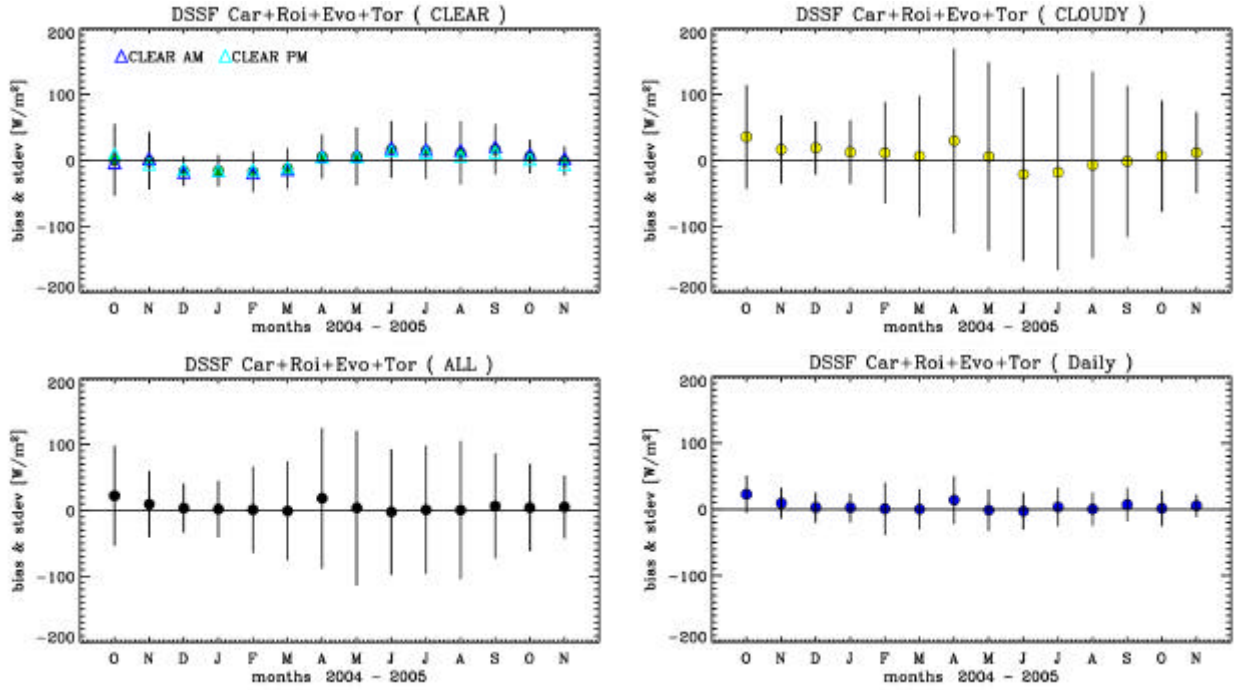

Figure 11: Temporal evolution of bias and standard deviation between the Land-SAF DSSF estimates and ground measurements for all validation stations combined (Carpentras, Roissy, Evora, and Toravere).

4. PERSPECTIVES

In general the validation results obtained so far show a good consistency with in-situ observations or equivalent products derived from other satellites. Nevertheless the present Initial Operational Phase still allows us to adjust the algorithms and implement some methodological improvements. In addition to continued validation studies we intend to test the application of the products in surface and NWP models in order to get a direct feedback for further development.

For the albedo algorithm minor adjustments of the narrow- to broad-band conversion relations may be required depending on the results of extended validation studies. In addition, the quality of the input information for the atmospheric correction scheme needs to be improved. In particular the presently employed climatology for the aerosol optical thickness should later be replaced by a

dynamic aerosol product in order to remove from the surface albedo time series potential spurious fluctuations caused by unaccounted atmospheric variability.

The directional-hemispherical albedo is given for a reference angle corresponding to the local solar noon. We plan to provide a parameterisation which enables the user to calculate the diurnal albedo cycle. In addition to the currently available albedo product, which is suitable for near real time applications, we also envisage the implementation of a variant with different temporal characteristics based on the accumulation of the observations acquired within a "classical" temporal composition window as depicted in the plot on the right in Figure 1. Such an approach is appropriate for example for deriving a climatology of the variables characterising the surface properties.

After the launch of the first satellite of the MetOp series, the data acquired by the AVHRR instrument onboard will also be processed and exploited by the Land-SAF system. Owing to the complementary observation geometry resulting from the polar orbit, the additional information will be particularly beneficial for the albedo product – provided that technical problems such as geo-location and channel inter-calibration can be controlled with sufficient precision. It is planned to merge the data at the level of the TOC-reflectance factor by inverting the BRDF model with observations from both the SEVIRI and AVHRR instruments. Especially for high latitudes during winter this will significantly improve the constraints for model inversion and hence the quality of the result.

Concerning the DSSF estimates for cloudy sky conditions there is still some room for improvement by fine tuning and adapting some of the parameters used in the algorithm or by exploiting additional information such as the cloud type. For clear sky we envisage to re-formulate the currently applied parameterisation as a function of the aerosol optical thickness for which we expect that a dynamic estimate will be available in the near future in the framework of other projects.

In addition to the presently available instantaneous flux estimates it is planned to implement a daily averaged or integrated product during the forthcoming project phase. By taking into account the observations delivered by the polar-orbiting system this product could be improved and extended towards high latitudes beyond the region covered by the Meteosat disk.

5. REFERENCES

Baseline Surface Radiation Network: http://bsrn.ethz.ch

Land-SAF, 2005, Land Surface Albedo, Product User Manual, Version 1.3

Land-SAF, 2006, Down-welling Surface Short-wave Radiation Flux, Product User Manual, Version 1.3

MODIS Albedo: http://www-modis.bu.edu/brdf

OSI SAF, 2002, Surface Solar Irradiance Product Manual, Version 1.2. http://www.osi-saf.org

CURRENT STATUS AND FURTHER DEVELOPMENTS OF THE VEGETATION PRODUCTS

F. J. García-Haro, F. Camacho-de Coca and J. Meliá

Remote sensing Unit, University of Valencia
C/Dr. Moliner, 50. 46100. Burjassot. València. Spain

ABSTRACT

Global estimates of fractional vegetation cover (FVC) and leaf area index (LAI) are necessary for Numerical Weather Prediction (NWP), regional and global climate modeling, weather forecasting and global change monitoring. The scientific user communities have expressed the need for timely series of these parameters, which are also relevant for a broad range of Biosphere Applications such as agriculture, forestry, environmental management and land use, hydrology and natural hazards monitoring.

In the framework of the EUMETSAT Land SAF the University of Valencia team is the responsible for the development of algorithms to obtain vegetation products, including the scientific validation of the products. The vegetation algorithms provide a principled statistical approach to spectral mixture analysis, which outperforms the common literature methods. They assume a signal from of a target (vegetation) and a background (soil). Both target and background are non Gaussian with unknown probability density function. The algorithm relies on a probabilistic method in which endmember signatures are no longer treated as constants, but they are represented by multi-modal probability density functions. The method shows to be effective in incorporating detailed information about the soil and vegetation conditions in the scene. The use of standardised signatures improves understanding of the impact of endmember variability on the derivation of subpixel vegetation fractions at a global scale.

Presently, the algorithms are running in the Land-SAF system over Europe, Africa and South America regions, producing daily FVC and LAI fields and their respective error estimates and quality flags. These products are already available via ftp to the beta user community. Multiple validation techniques are used to develop uncertainty information on vegetation products. Early validation results indicate the soundness and reliability of the Land SAF FVC and LAI products from both perspectives, spatial and temporal. An inter-comparison with similar products has shown the statistical consistency between products at the level of individual pixels, representative core sites, biome types and geographical areas.

1. INTRODUCTION

The FVC (Fractional Vegetation Cover) and LAI (Leaf Area Index) and the fraction of Absorbed Photosynthetically Active Radiation (fAPAR) are important structural properties of land surface areas occupied by plant canopies. The FVC characterizes the fraction of vegetation on a flat background covered by vegetation. The LAI is a dimensionless variable [m^2/m^2] defined as one half the total leaf area per unit ground area and accounts for the surface of leaves contained in a vertical column normalized by its cross-sectional area. The fAPAR represents the fraction of the solar energy which is absorbed by vegetation for photosynthesis.

The FVC determines the partition between soil and vegetation contributions for further estimates of total emissivity and temperature. This product is mandatory for a thorough description of land surface processes in the surface parameterisation schemes implemented in the climate and weather forecasting models. For fully and healthy developed canopies, the LAI indicates the amount of green vegetation that absorbs or scatters the solar radiation in determining the characteristics of the remote sensing signal. It represents the interface between the soil background and the atmosphere for the energy and mass exchanges. The LAI is a key input of Numerical Weather Prediction (NWP) models, regional and global climate modelling, weather forecasting and global change monitoring. The fAPAR is an indicator of the health and thereby productivity of vegetation. Besides, the FVC, LAI and fAPAR are relevant for a wide range of Land Biosphere Applications such us agriculture and forestry, environmental management and land use, hydrology, natural hazards monitoring and management, vegetation-soil dynamics monitoring, drought conditions and fire scar extent.

This contribution has been developed in the frame of the LSA SAF Project (Satellite Application Facility on Land surface analysis), which is part of the ground segment for the future EUMETSAT missions METEOSAT Second Generation (MSG) and European Polar System (EPS). The University of Valencia team is the responsible for the development and implementation of algorithms to obtain FVC and LAI products from SEVIRI/MSG and AVHRR-3/EPS data. These products will provide a characterisation of the state of vegetation, offering a number of advantages of primary importance for meteorological, climate and biosphere modelling. First, it is a global dataset and consequently the problems of lack of homogeneity associated to the usage of different databases are circumvented. Second, the high rate of acquisition guarantees the availability of spatially consistent cloud-free data. Third, temporal information about the seasonality of vegetation is provided due to the frequent repeat cycle. Fourth, it offers cost-effective data handling requirements for global scale studies.

Section 2 describes briefly the algorithm proposed to estimate the FVC and LAI. The current status of the vegetation products is summarized in section 3. Finally, sections 4 and 5 address the scientific validation of the products and ongoing activities.

2. ALGORITHMS AND METHODS

In the last few years, methodologies have been developed to estimate land surface bio-physical parameters from large scale optical sensors in an operational way. These algorithms have been implemented in operational processing line to provide advanced bio-physical products from POLDER (Leroy et al. 1997, Roujean and Lacaze 2002), MODIS and MISR (Knyazikhin et al. 1999) and MERIS (Gobron et al. 1999, Baret et al. 2003).

Many available global maps used in climate and NWP still depend on land cover classifications or are based on correlation between vegetation properties and simple spectral indices. These methods may lead to inaccurate estimates of vegetation cover due to the complex spatial patterns of sub-pixel vegetation cover. The process of identifying the sub-pixel proportions of the constituent components is called spectral mixture analysis (SMA). This is a widely used method to determine the sub-pixel abundance of vegetation, soils and other spectrally distinct materials. Mixture modelling approaches are methods especially adequate for global studies, since the spatial variability within pixel is high. A variety of studies have supported this assumption on a number of space-borne sensors, including TM, VEGETATION and MODIS. The SMA methods have demonstrated an improvement in FVC and LAI estimates when compared to predictions using standard spectral vegetation indices.

The effectiveness of the linear mixture model is dependent on the degree of separation of the different signatures, as well as the level of noise which is present in the scene. This imposes clear limits on the number and similarity of the land cover classes that can be reliably distinguished. The intra-species spectral variability, lighting and topographic effects, uncertainty related to apparent surface reflectance retrievals, and noise in field or image endmembers are sources of uncertainty that compromise the ability to retrieve relevant information using SMA (García-Haro et al. 2005a).

The algorithm to estimate the FVC is aimed at reducing the bias due to the above problems. It assumes a signal from of a target (vegetation) and a background (soil). Both target and background are non Gaussian with unknown probability density function. Figure 1a illustrates a schematic representation of the problem in a two-dimensional features space, e.g. the red-NIR space. Both vegetation and non-vegetation classes are represented by a multi-modal distribution attributable to differences due to biophysical and biochemical composition. Rather than a single signature to represent a certain vegetation species or soil type, its entire variability is accounted for by using Gaussian probability densities. This addresses more reliably the pixel deviations from its expected value due to the natural variability of the scene materials. The algorithm uses the Expectation-Maximization (E-M) approach to estimate the individual Gaussian components, which shows to be an efficient method when the number of Gaussians is defined beforehand (Fraley and Raftery, 2002).

At a coarse spatial resolution, any point in the vegetation region can combine with another point in the non-vegetation region to produce a mixture signal. Hence, the algorithm assumes that each unknown pixel can be modelled as a sum of candidate models (i.e. pairs of vegetation and soil subclasses). In this sum, the contribution of each model is weighted by its Bayesian *a posteriori* probability. The local probabilities from the various candidate model mixtures is used to identify not only the mixture proportions in the mixed pixel, but the confidences assigned to them.

Rather than using reflectance, the algorithm uses as input the k_0 coefficient of the BRDF model for the different spectral channels (Geiger et al. 2004) in the three relevant SEVIRI spectral channels: red (VIS-0.6), near-infrared, (NIR-0.8) and middle-infrared, (SWIR-1.6). Physically the k_0 parameters correspond to isotropic reflectance, i.e. reflectance factor values directionally normalized to reference illumination and observation zenith angles of 0°. This geometry leads to a minimum contribution of the shadow proportion (hotspot geometry) and a physically correct estimation of FVC (Roujean and Lacaze 2002), coinciding with the complement to unity of the gap fraction at nadir direction. Since green vegetation strongly absorbs solar radiation in the red spectral region, and strongly scatters it in the NIR, these two bands are widely used to characterize land surfaces from remote sensing data. The algorithm uses also SWIR information, which provides useful information about the vegetation water content and mitigates the inaccuracy caused from saturation phenomena in estimating vegetation coverage. Moreover, this channel exhibits a large degree of sensitivity to changes in LAI (Eklundh *et al.*, 2001). In the features space

of the red-NIR-SWIR channels, the soil/vegetation components are spectrally distinct enough and the bands are sufficiently uncorrelated.

Figure 1b allows understanding better the physical basis of the algorithm and provides further details of its performance. Ellipses are projections of the ellipsoids defined by the covariances of the soil/vegetation Gaussian components onto the $k_{0,red}$ - $k_{0,NIR}$ features space. The FVC isolines (lines connecting points of identical FVC) range from 0 to 1 FVC values at 0.04 spacing intervals. The algorithm outperforms the common SMA approaches since:

1. It has the ability to generalize valuable information ingested from an exhaustive training data set, which combines a variety of data sources (global land cover classifications, satellite products and fine resolution satellite data).
2. The isolines capture the essential relationship between reflectance and FVC, showing a general agreement with literature studies (e.g. Huete et al. 1988).
3. There is a gradual change in FVC reflectance along the "reflectance triangle". This partly reduces errors due to input noise, since these errors are proportional to the local gradient of FVC in the features space.
4. The use of standardised SMA improves understanding of the impact of endmember variability on the derivation of subpixel vegetation fractions at a global scale.
5. The probabilistic approach provides a means to quantitatively assess the FVC error, which addresses the uncertainty due to the model selection and the propagation of the input errors.

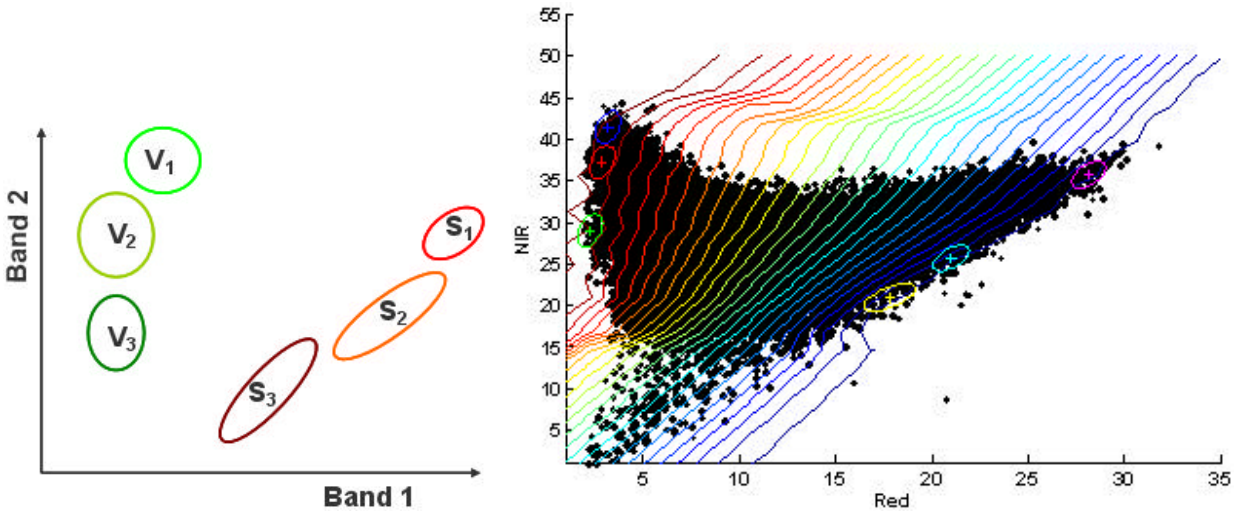

Figure 1: (a) Simplified illustration of the parameterization of the background (S) and target (V), from a mixture of Gaussians (clusters). The ellipses represent the isolines of the Gaussian functions, i.e. feasibility regions on the spectra of the constituents due to the natural variability in the material itself and other effect such as atmospheric/illumination conditions and data noise. (b) Typical pattern of the FVC in the red-NIR space.

FVC is subsequently used to generate estimates of LAI (Roujean and Lacaze 2002):

$$FVC = a_o\{1-\exp(-b\cdot G(q_s)\cdot\Omega\cdot LAI\} \quad (1)$$

where *b*, equal to 0.945, is a function of the leaf albedo (Roujean, 1996); $G(q_s)$ is the leaf projection factor (Ross, 1981), here assumed to be equal to 0.5 for a spherical orientation of the foliage; a_0 is

a coefficient in the range (1.03-1.08); Ω is the clumping index (Nilson, 1971) which accounts for the degree of dependence of the vegetation stands position and is assumed to be biome-dependent (Chen et al. 2005). This method has consistently proven to be more effective than traditional remote sensing techniques that use unadjusted spectral vegetation indices (Peddle *et al*., 2001; Hu *et al.*, 2004).

3. PRODUCT DESCRIPTION

Presently, the FVC and LAI SEVIRI vegetation products relies on the albedo and BRDF cloud-cleared TOC BRDF k_0 parameter in the VIS-0.6, NIR-0.8 and SWIR-1.6 SEVIRI channels. The temporal and spatial resolution of the vegetation products are tied to those of BRDF product, which is currently produced at a daily basis using an iterative scheme with a characteristic time scale of five days (see details in the Albedo Product User Manual).

Considerable attention has been paid to implement a set of quality control protocols that help users match data sets to their applications. Quality control measures are currently produced at the pixel level. Quality control information is represented by the error estimate and the quality flag separate data layers in the HDF5 file whose pixel values correspond to specific quality scoring schemes. The details of the quality flag information for FVC and LAI are given in the vegetation Product User Manual document. The products and their respective error estimate are produced using the signed 16-bit integer variable. The quality control variables are 8-bit unsigned integer measures without a gain or offset. The product files also contain a considerable amount of extra information (classic metadata) that describes various properties of the data.

Dataset name	Unit	Range	Variable Type	Scale Factor
FVC	1	[0, 1]	2-Byte Signed Integer	10000
FVC err	1	[0, 0.2]	2-Byte Signed Integer	10000
Quality Flag	na	[0,255]	1-Byte Unsigned Integer	na

Table 1: Content of the FVC product.

Dataset name	Unit	Range	Variable Type	Scale Factor
LAI	1	[0, 7]	2-Byte Signed Integer	1000
LAI err	1	[0, 1.5]	2-Byte Signed Integer	1000
Quality Flag	na	[0,255]	1-Byte Unsigned Integer	na

Table 2: Content of the LAI product.

Figure 2 shows an example of SEVIRI FVC and LAI products corresponding to 15th August 2005, as obtained with the last code version (v1.2). These products have been produced from the day one of production of AL2 products version 5.0 (2 August 2005).

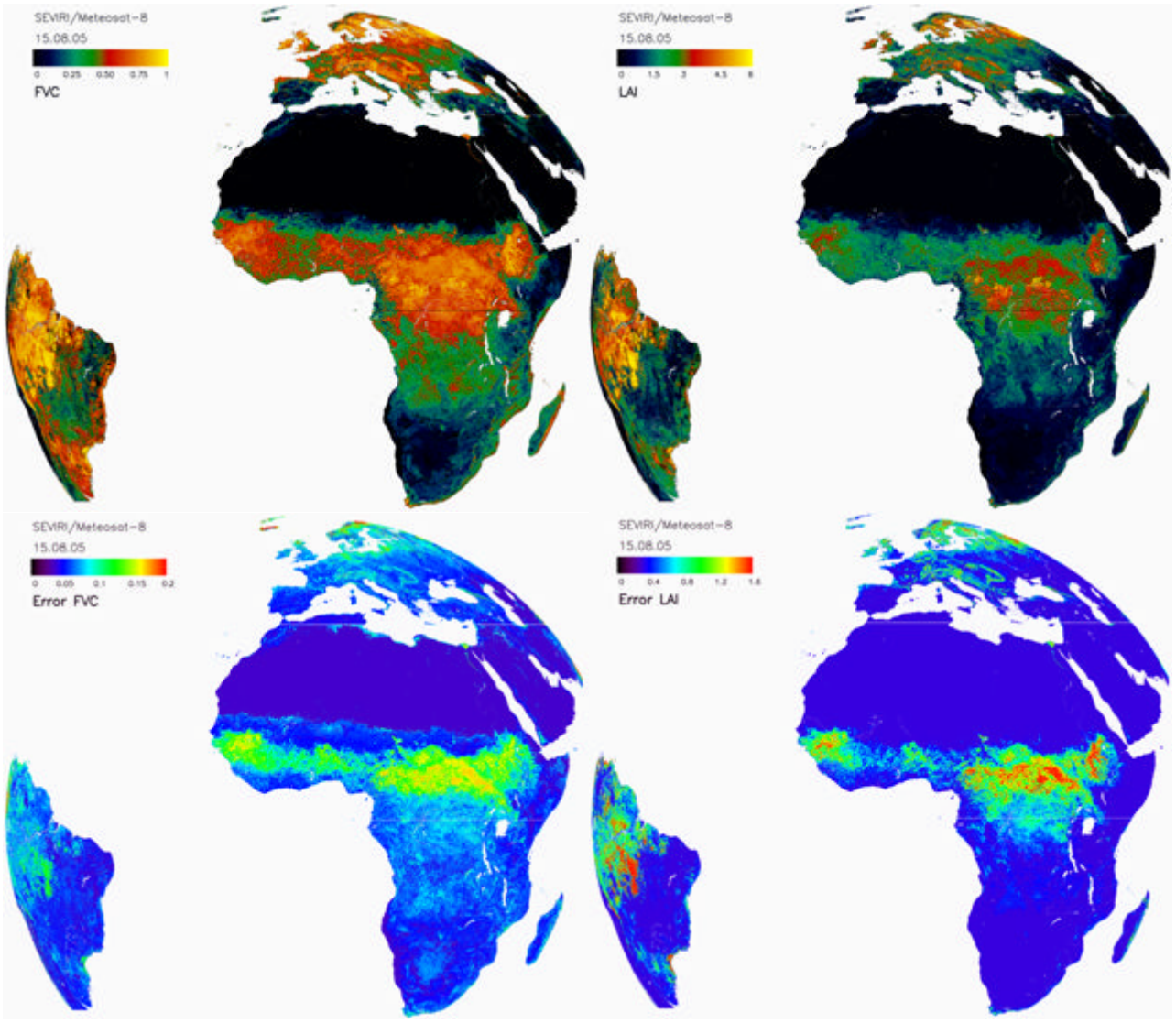

Figure 2: FVC (left) and LAI (rigth) product composition of the four LSA SAF geographical areas corresponding to the 15th of August 2005. Top correspond to products and bottom to associated error estimates.

Visually, the FVC is spatially consistent and shows a high coherence with the available ground truth. In general, the FVC confidence is the lowest at high latitude regions, since the quality of the inputs is significantly poorer. The outputs present practically no missing data except for areas which are usually covered by snow. The variations are generally higher at high latitudes and over tropical latitudes (e.g. over broadleaf forests) where there is frequent cloud cover. Nevertheless, FVC and LAI profiles are relatively clean, with low residual contamination due to atmosphere (aerosols), clouds or soil effects. Small variations are generally found for retrievals from observations with temporal proximity (days). This result is coherent with the slow variations in physical condition (properties) of land cover on a SEVIRI time resolution over a period of several days. The causes of variations in LAI values are due to changes in the atmosphere and the undetected presence of cloud contamination and snow cover.

All observations declared as snow-free over land by the BRDF albedo algorithm are processed. However, there is evidence that in some cases snow or water contaminated pixels are not effectively removed, which may lead to biases in the resulting FVC estimates. The algorithm

identifies pixels that are likely to present a significant contribution of inland water, snow or abnormally dark spectra (which are likely to be noisy). They are not processed since it would significantly deteriorate the quality of the product. The products should be used with caution in view of changes to calibration, geolocation, cloud screening, atmospheric correction and ongoing validation activities. In particular, the users are advised to pay attention to the quality flag files accompanying the products.

4. SCIENTIFIC VALIDATION

As specified in the User Requirements Document the objective for the accuracy of vegetation products is 15% using SEVIRI/MSG data. Different prototyping exercises (either using POLDER/ADEOS or VEGETATION/SPOT data) have shown that the FVC and LAI fields retrieved using the Land-SAF algorithm are temporally consistent and show overall uncertainty (RMS) similar to equivalent products and products derived using operational algorithms, ranging from about 0.1 for FVC and 0.8 for LAI (Camacho-de Coca et al. 2005; García-Haro et al. 2005b).

Scientific validation is the only way to assess the uncertainty of the satellite products. However, this is a challenging task especially at the coarse SEVIRI scale, since field campaigns are limited in time and space. Currently, VALERI, CEOS-LPV and MODLAND sites are a good example of international effort in this direction. Reliable field information is available since 2000. Some of these sites such as BELMANIP (Baret et al. 2006) and MODLAND (Morisette et al., 2002) have been selected mainly for temporal consistency assessment of vegetation products. Multiple validation techniques are used to develop uncertainty information on vegetation products. Three main activities are currently considered: (i) direct validation with ground-truth, (ii) indirect validation against reference products and (iii) consistency analysis with other Land-SAF products. Indirect validation or inter-comparison exercises are the best way to assess the spatial and temporal consistency of the Land-SAF products regarding equivalent satellite products, although such evaluation is always in relative terms. Different coarse resolution satellite products (MODIS, POLDER, VEGETATION) derived from different methodologies have been used as reference FVC and LAI values. The strategy adopted for confirming the achievement of the validation and some preliminary results are documented in the Scientific Validation Plan Document.

Preliminary validation activities indicate the soundness and reliability of the Land-SAF FVC and LAI products from both perspectives, spatial and temporal. The analysis of consistency and temporal trends has mostly focussed on the summer and autumn 2005 period. The trend of FVC and LAI are temporally stable and coherent with expectations. This is a further confirmation that the products respond well to vegetation changes provoked by seasonal activity of vegetation. In addition, the comparison of LAI-SEVIRI products with upscaled insitu measurements performed during the SEN2FLEX ESA campaign carried out at the Barrax site during July 2005 reveals an acceptable correspondence (RMS=0.34, r= 0.62).

Indirect validation activities have focussed on the intercomparison analysis of SEVIRI products with equivalent MODIS, POLDER and VGT products. An example of this analysis is shown in figure 3. It reveals a good agreement between daily SEVIRI-LAI and MODIS LAI-8day (MOD15A2 product) over different MODLAND core sites situated in Europe and South Africa. The correspondence between SEVIRI and MODIS reference product is noticeably high in the South Africa region.

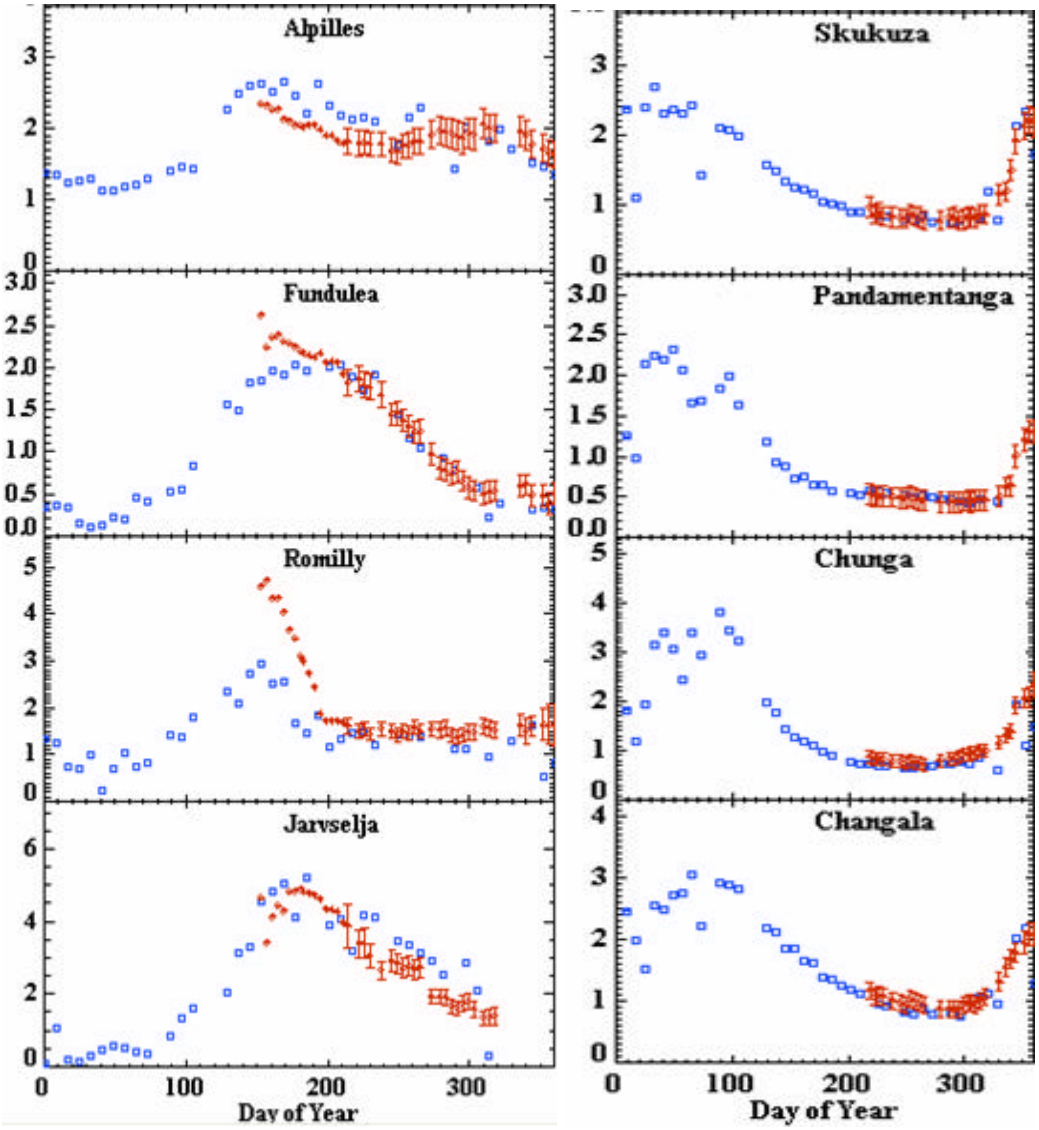

Figure 3: Time series of MODIS-8day and SEVIRI v1.2 daily LAI products for the MODLAND areas (200x200 km) over Europe and South Africa. In order to enhance the clarity, only every fourth daily estimate and error bar is plotted. Missing data correspond either to days for which albedo inputs were not generated or to days for which the outputs can not be calculated (usually due to the snow cover). The error bars of SEVIRI products are only available since August 2005.

5. CONCLUDING REMARKS AND PERSPECTIVES

Presently, the algorithms are running in the Land-SAF system and producing daily FVC and LAI SEVIRI fields over Europe, Africa and South America regions along with their respective error estimates and quality flags. These products are available in HDF5 format via ftp. The evaluation of the products by the beta user community will serve to gain further confidence before declaring these products as pre-operational. Potential applications of these products will also be promoted in close collaboration with users.

In overall, the products have shown to be statistically consistent with similar products at the different levels: individual pixels, representative core sites, biome types and full SEVIRI geographical areas. It is found that the deviations from reference ground and satellite products lie

well under the baseline of the uncertainty ranges that obtained when comparing different reference products. Validation work will continue to provide a medium and long-term assessment of the product quality in a systematic and statistically robust way representing global conditions. The development and operational implementation of the fAPAR product is envisaged for 2006. The basis will be the Roujean and Bréon (1995) algorithm, which relies on the BRDF at an optimal configuration.

Further developments will exploit the full angular capabilities provided by SEVIRI/Meteosat and AVHRR/Metop data, which will allow a directional spectral mixture analysis (García-Haro et al. 2006) to be implemented. The algorithm maintenance activities will be focused on the improvement of the description of land surface properties, more detailed and accurate land cover classification (e.g., GLOBCOVER), more accurate parameterization of clumping index used in the algorithms, and a more detailed and accurate product quality control.

6. BIBLIOGRAPHIC REFERENCES

BARET , F.,C. BACOUR, and G. DERIVE, (2003). From Level3A to LAI, fAPAR and fCover biophysical products. ATBD CYCLOPES V1.

BARET, F., J: MORISSETTE, R. MYNENI, R. FERNANDES, J. CHEN, S. PLUMMER, J.L. CHAMPEAUX, M. Weiss, G.DERIVE and C. BACOUR, (2006). Evaluation of the representatitvity of networks of sites for the validation and inter-comparison of global land biophysical products. Proposition of the CEOS-BELMANIP. IEEE Special issue on Validation and accuracy assessment of global products. (in press).

CAMACHO-DE COCA, F., F.J. GARCÍA-HARO, R. LACAZE, M. LEROY, J.-L. ROUJEAN and J. MELIÁ (2005). *Validation of the LSA SAF FVC and LAI prototype algorithm with POLDER/ADEOS data over Western Europe.* EUMETSAT Meteorological satellite conference, Dubrovnik, Croatia, 19-25 Sept 2005 (in press).

CHEN , J. M., C. H. MENGES, S. G. LEBLANC, 2005, Global mapping of foliage clumping index using multi-angular satellite data, Remote Sensing of Environment, 97: 447 – 457

EKLUNDH, L., HARRIE, L., & KUUSK, A. (2001). Investigating relationships between Landsat ETM+ sensor data and leaf area index in a boreal conifer forest. Remote Sensing of Environment, 78, 239–251.

FRALEY, C., & RAFTERY, A. E. (2002). Model based clustering, discriminant analysis and density estimation. Journal of the American Statistical Association, 97, 611 – 631.

GARCÍA-HARO, F.J, S. SOMMER, T. KEMPER (2005a), Variable multiple endmember spectral mixture analysis (VMESMA), *International Journal of Remote Sensing*, 26:2135-2162.

GARCÍA-HARO, F.J., F. CAMACHO-DE COCA, J. MELIÁ, B. MARTÍNEZ, Operational derivation of vegetation products in the framework of the LSA SAF project, (2005b), EUMETSAT Meteorological Satellite Conference. Dubrovnik (Croatia). 19-23 Septiembre, in press.

GARCÍA-HARO, J, F. CAMACHO-DE COCA y J. MELIÁ, (2006). A directional Spectral Mixture Analysis. IEEE Transactions on Geoscience and Remote Sensing, vol 4, no.2, February 2006 (in press).

GEIGER, B. L. FRANCHISTEGUY, and J.L. ROUJEAN, (2004), Land Surface Albedo from Meteosat Second Generation (MSG) Observations, IGARS, in press.

GOBRON N., B. PINTY, M. VERSTRAETE, and Y. GOVAERTS (1999). The MERIS Global Vegetation Index (MGVI): description and preliminary application. *Int. J. Rem. Sensing*, 20:1917-1927.

HUETE, A.R. (1988). A Soil Adjusted Vegetation Index (SAVI). Remote Sens Env. 25:295-309.

HU, B., MILLER, J., CHEN, J. AND HOLLINGER, A. 2004. Retrieval of the Canopy LAI in the BOREAS Flux Tower Sites Using Linear Spectral Mixture Analysis. Remote Sensing of Environment 89: 176-188.

KNYAZIKHIN, Y., J. GLASSY, J.L. PRIVETTE, Y. TIAN, A. LOTSCH, Y. ZHANG, Y. WANG, J.T. MORISETTE, P. VOTAVA, R.B. MYNENI, R.R. NEMANI, and S.W. RUNNING, (1999), MODIS leaf area index (LAI) and fraction of potosynthetically active radiation aborbed by vegetation (FPAR), Product (MOD15) ATBD.

LEROY, M., J.L. DEUZÉ, F.M. BRÉON, O. HAUTECOEUR, M. HERMAN, J.C. BURIEZ, D. TANRÉ, S. BOUFIÈS, P. CHAZETTE et J.L. ROUJEAN, Retrieval of atmospheric properties and surface bi-directional reflectances over the land from POLDER/ADEOS, *Journal of Geophysical Research, 102, 17,023-17,037*, 1997.

MORISETTE J.T., PRIVETTE J. L., JUSTICE C.O (2002). A framework for the validation of MODIS land products. *Remote Sensing of Environment*, 83(1-2), 77-96.

PEDDLE, D. BRUNKE, S. and HALL, F. 2001. A Comparison of Spectral Mixture Analysis and Ten Spectral Vegetation Indices for Estimating Boreal Forest Biophysical Information from Airborne Data. Canadian Journal of Remote Sensing 27 6:627-635.

ROUJEAN, J.L. and R. LACAZE, (2002). Global mapping of vegetation parameters from POLDER multiangular measurements for studies of surface-atmosphere interactions: A pragmatic method and its validation. J. Geophysical Res., 107D, 10129-10145.

ROUJEAN, J.L., and F.M. BRÉON, (1995), Estimating PAR absorbed by vegetation from bidirectional reflectance measurements, *Remote Sensing of Environment*, 51:375-384.

VALIDATION OF LSA-SAF SNOW COVER PRODUCT

Niilo Siljamo

Finnish Meteorological Institute, Earth Observation
P.O.Box 503, FI-00101 Helsinki, Finland

ABSTRACT

MSG SEVIRI satellite data is used to produce daily LSA SAF Snow cover pre-operationally at Instituto de Meteorologia, Portugal. The LSA SAF Snow cover product is a simple classification of each SEVIRI pixel to snow free, partially snow covered or totally snow covered category. Algorithm is using all SEVIRI channels. The snow cover is produced each repeat cycle (15 min) throughout the day. These single scene snow cover fields are combined to produce daily snow cover field. The SC product was developed by Swedish Hydrological and Meteorological Institute (SMHI). Finnish Meteorological Institute (FMI) has the responsibility of the product development and maintenance since the beginning of 2005.

Validating satellite based snow cover with in situ measurements is extremely demanding. Best possible choice is to use standardised surface observations from large geographical areas. Synoptic weather stations observe snow depth at least daily all over Europe. These observations are used to validate the daily LSA SAF snow cover product.

The SC product is available from 1st February 2005. For this analysis SYNOP observations and ECMWF snow analysis are retrieved from the ECMWF MARS database for the period from October 1st 2005 until February 1st 2006. This data covers almost all of Europe reasonably well. There are some areas where snow depth observations are rare or missing.

In general the SC product and observations are in good agreement, especially if partial snow cover is considered as snow covered. During the winter 2005-2006 60541 individual observations could be used to validate the snow cover product. The correlation between surface observations and LSA SAF Snow cover was 0.56. LSA SAF Snow cover product and SYNOP observations were in agreement at 84\% of compared observations. False positive rate was 1.4\% and false negative rate 14.9\%. Further work is needed to detect problematic conditions for snow detection. These could include forests, mountains and areas where snow cover is varying rapidly.

Some improvements to the LSA SAF Snow cover algorithm are planned. The snow cover can be detected from satellite using visual channels only in cloud free areas. The NWC SAF cloud mask is developed to detect cloudy pixels instead of cloud free pixels. When compared to SYNOP cloud observations it was found that cloudy pixels were observed correctly but there were serious

limitations in the detection of cloud free pixels. For this reason a more direct algorithm to detect snow cover will be developed.

1. INTRODUCTION

Satellite remote sensing of the snow cover is valuable method for mapping the snow cover in large areas. It is quite demanding to detect snow on the surface when clouds, vegetation and varying light conditions change the observation conditions.

Currently pre-operational daily LSASAF snow cover product was developed by SMHI. It is based on NWCSAF Cloud mask data, which has its limitations due to its purpose. Results are reasonable, but there is still need for improvements. An example of SC product can be seen in the Figure 1. It is obvious that some snow covered areas are not detected by the SC algorithm, but in general the snow covered area is detected correctly.

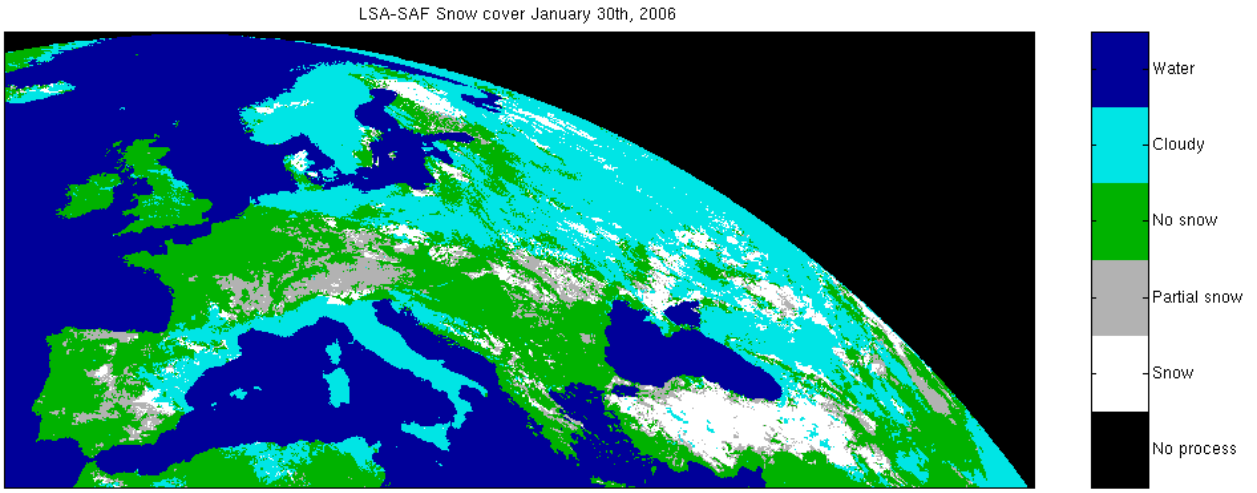

Figure 1: LSA-SAF Snow cover for January 30th 2006. Green areas are snow free, grey and white areas are snow covered. It can be seen that some snow covered areas are not detected. For example all of Finland is snow covered at end of January.

FMI got the algorithm maintenance and development responsibility at the beginning of 2005. In the future versions of the snow cover algorithm the satellite data will be used directly. This should improve the accuracy of the SC product.

2. EXAMPLES OF SNOW COVER

The problems of remote sensing of snow cover can be illustrated by photographs of actual snow cover. During the snow season rapid changes of the snow cover are probable. Snow free areas can be covered by snow in just few hours. During the melting season the properties of the snow change during the day.

New snow and old, perhaps partially melted snow, are different. Frost and frozen dew might cover large areas. New snow on warm ground or wetlands can change to slush or other mixtures of snow and water. Lakes and rivers can freeze and be covered by snow.

In forest areas the ground can be covered by thick layer of snow, which can be difficult to detect from satellite, especially in evergreen forest areas. The trees can also be covered by snow, which can fall off when the weather conditions change and lead to rapid changes in the apparent snow

cover. Other vegetation types can also change the appearance of the snow cover and change the surface albedo. The effect of tree shadows in forest areas must be considered.

Clouds are the most significant problem when satellite data is used for snow detection. It is impossible to see the surface under the clouds in visual channels. Other effects caused by the clouds are the cloud shadows which change the lighting conditions on ground. Also the viewing angle and solar angle change the view.

Lighting conditions together with topography create a demanding task when detecting the snow cover in mountain regions.

In the Figure 2 many of these problems can be seen. Clouds, shadows, trees and other vegetation make the surface quite complicated to classify as snow free or snow covered without intelligent observer.

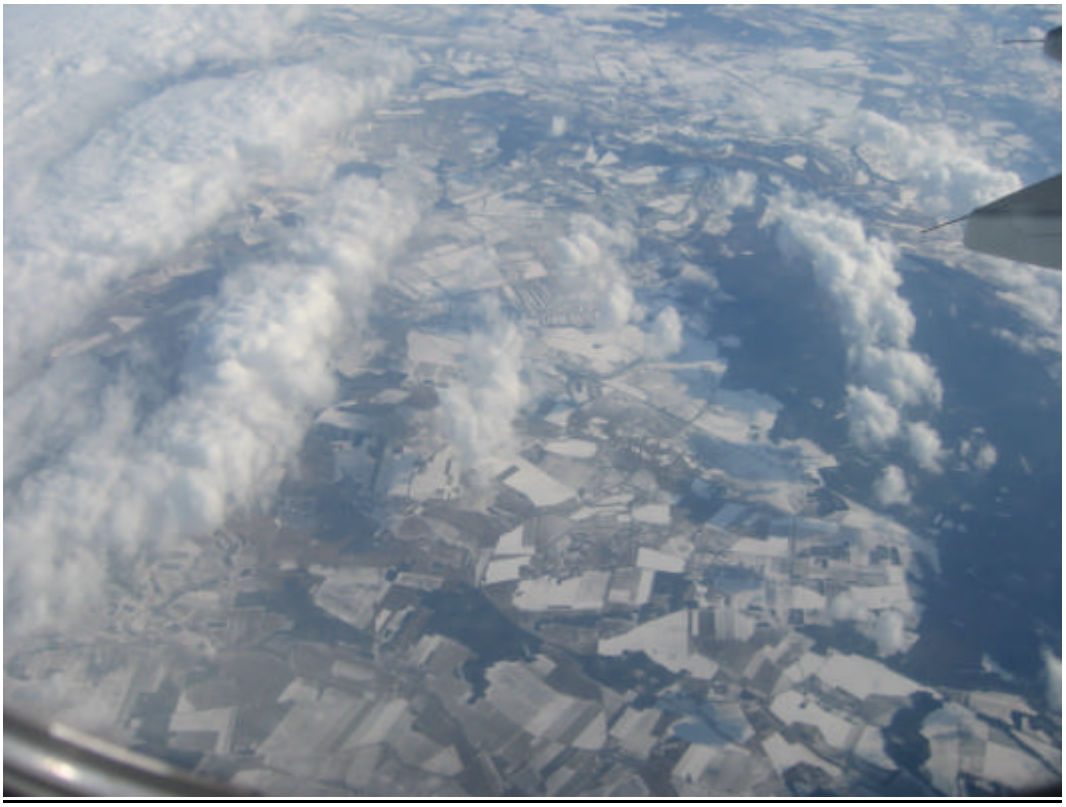

Figure 2: Snow cover seen from air above southern Germany. This photograph shows several features which must be considered when developing snow detection algorithms. The surface can not be seen under the clouds. Near the clouds can be seen the shadows of the clouds. All of the area is snow covered, but forests and vegetation on the fields hide the snow in large areas.

Rapid change of the snow cover is illustrated by the pair of photographs in Figure 3. Just after the snowfall the ground and trees are covered by snow. This kind of postcard view is typical during the winter in the northern Europe. When the weather changes, the snow falls off from the trees and bushes and this changes the properties of the snow cover. If the weather is cold and calm the snow can stay on the trees several weeks.

Figure 3: Rapid change during the winter. On the top can be seen fresh snow just after the snowfall. The snow covers the entire surface and some snow is also on trees and bushes. The snow cover can stay like that just few hours or even weeks, but then the change is usually quite rapid. In just few hours the snow falls of the trees and the scenery changes (below). Helsinki, Finland

Sometimes the ground is covered by frost or frozen dew (Figure 4), typically after a cold night. Usually frozen dew melts a few hours after the sunrise, but before that it has a significant effect on the radiative properties of the ground surface, e.g. albedo. If the snow product is used for hydrological purposes, the effects of frost and frozen dew on snow cover classification must be eliminated.

Figure 4: Frost on ground in the cold morning. The ground and especially grass is covered by small ice crystals. In this case just the lowest few meters of the air were below freezing point, but when the cold layer covers also the trees, frozen dew can cover the trees. Helsinki, Finland

Trees can be covered by snow. Quite often the snow on trees falls off in a few days, but sometimes forests can be snow covered several weeks. The ground under the trees can be covered by snow, but often the snow depth in the forests is smaller than in the open areas (Figure 5). The trees can obscure the snow under the trees, especially in coniferous evergreen forests which are quite common in the northern parts of Europe. In the high latitudes low solar angles create often long shadows, which can also be seen in the Figure 6.

During the winter more and more of frozen dew and snow can accumulate on the trees. In certain conditions the snow can cover the trees completely in heavy snow. The forests covered by this kind of snow (Figure 7) should be classified as totally snow covered. The shadows of the trees can be clearly seen and this effect must be taken in account in the algorithm development.

During the melting season the properties of the snow cover change. During the night the temperature is lower and the water in the snow is freezing. During the day solar radiation and higher temperatures melt the snow. Typically after the winter the sun is warming trees and other objects which are not covered by snow. The melting is faster around these objects and this leads to typical pattern of snow free patches around trees and shrubs (Figure 8). During the melting season these areas should be classified as snow covered until the fraction of snow is below some predefined limit.

In the spring the snow on south sloping surfaces melt faster and for that reason the pattern of snow and snow free areas changes also in larger scale.

Figure 5: Snow covered trees in Luvia, Finland. These fir trees are covered by small amount of snow. The ground under the trees has a thin snow layer.

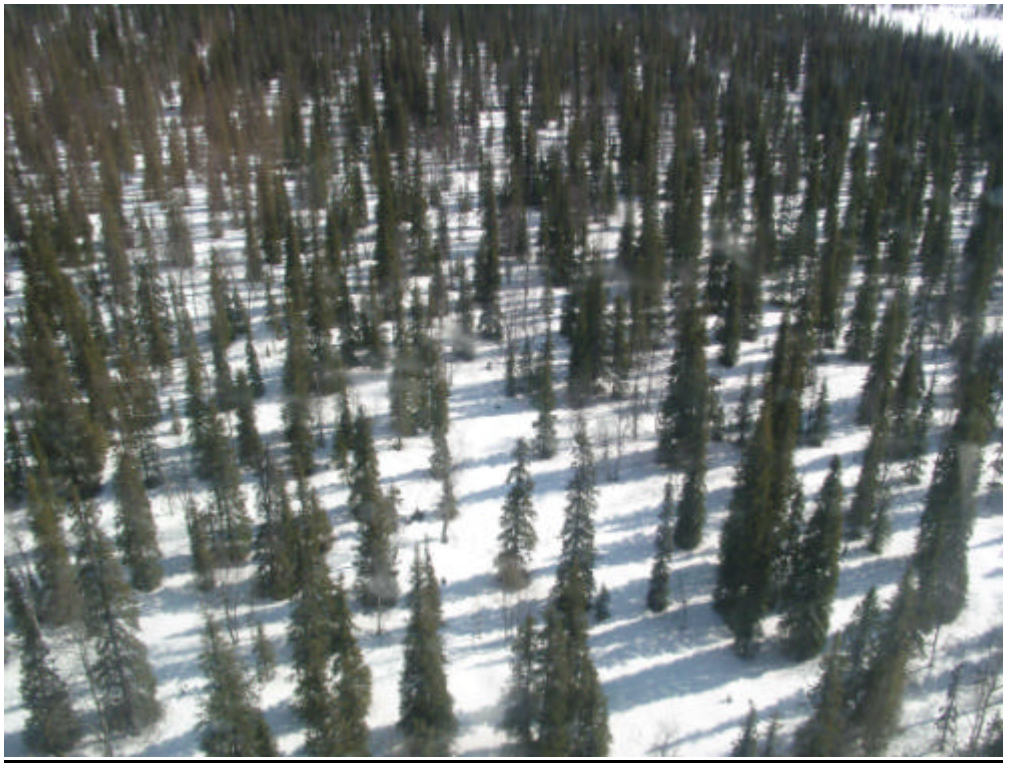

Figure 6: Shadows of the trees. The effect of the shadows of the trees can be seen clearly. The forest itself is quite sparse, but the shadows cover much of the area between the trees. Lapland, Finland

Figure 7: Heavy snow on trees, "Tykky" in Finnish. The area is totally snow covered and even the trees are covered by snow. Kuusamo, Finland. (Photo by Hilkka Pellikka/Wikimedia Commons)

Figure 8: Aapa mire during the melting season. Snow free patches can be seen around the trees, but the area is still mostly covered by snow. Lapland, Finland

3. LSA-SAF SNOW COVER ALGORITHM VALIDATION

Validating satellite based snow cover with in situ measurements is extremely demanding. Best possible choice is to use standardised surface observations from large geographical areas. Synoptic weather stations observe snow depth at least daily all over Europe. These observations are used to validate the daily LSA SAF snow cover product.

An example of the distribution of SYNOP snow depth observations in Europe is presented in the Figure 9. Although snow depth is a clear indication of presence of snow in an area, it does not give any information about the distribution of the snow. The snow cover can be patchy and unevenly distributed especially during the melting season.

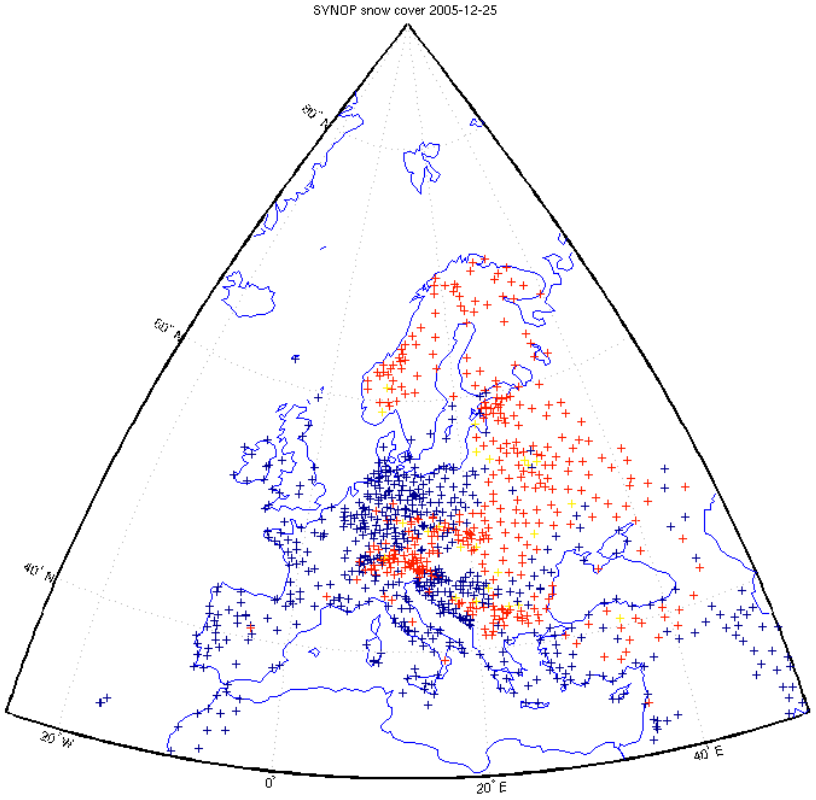

Figure 9: SYNOP weather station snow depth observations December 25th 2005. The stations which did not observe snow are indicated by blue markers. The stations which had at least some snow are marked by red or yellow.

For this comparison a period from October 1st 2005 until February 1st 2006 was selected. Snow depth observations from SYNOP weather stations were retrieved and these were compared to LSASAF SC product classification in the nearest pixel. During this period 60541 observations were available. The comparison results are presented in the Table 1.

Most of the observations are from snow free areas of which only 818 are false positive classifications. In the snow covered areas the results show that the algorithm needs further development, because just about half of snow covered pixels are correctly classified.

The NWC SAF cloud mask is developed to detect cloudy pixels instead of cloud free pixels. When compared to SYNOP cloud observations it was found that cloudy pixels were observed correctly but there were serious limitations in the detection of cloud free pixels.

The reasons for the inaccuracies in the classification need further research, although it is expected that direct use of MSG and other satellite data will improve the snow cover product. Most probable reason for misclassifications is vegetation, especially forests. Other possible reasons for classification problems might be mountains and rapidly changing snow cover. It is also possible that clouds and snow are not correctly classified in all cases.

Figure 9 shows that during the snow season the algorithm produce quite consistent results, although it seems that at the end of the period the fraction of correctly classified snow cover areas is a little smaller.

	SYNOP: snow	SYNOP: no snow
LSASAF SC: snow	7442 (12.29%)	818 (1.35%)
LSASAF SC: no snow	9001 (14.87%)	43280 (71.49%)

Table 1: LSA SAF Snow cover product compared to snow observations from SYNOP weather stations from October 1st 2005 until the beginning of February 2006. .

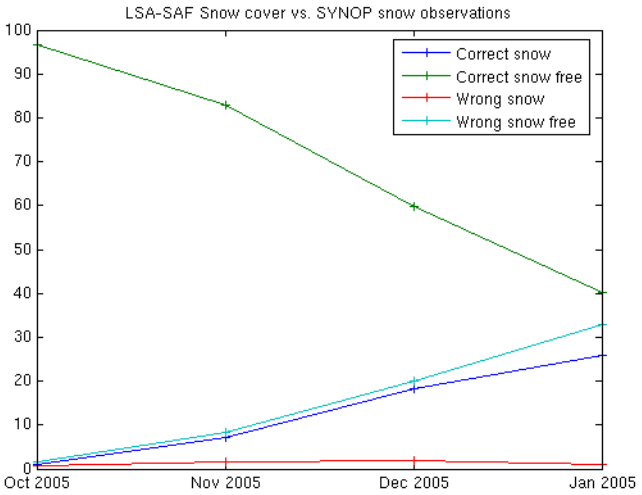

Figure 10: Behaviour of the LSASAF snow cover product during the winter.

4. CONCLUSIONS

The LSASAF Snow cover is pre-operational daily product. The comparison between SC product and weather stations snow depth observations show that the SC product is promising but further research is needed to improve the accuracy of the classification. The detection of snow is an extremely demanding task, because the snow cover is changing constantly and has lots of variations in different scales. The example cases present some of the potential variability of the snow cover and problematic conditions of during the snow season.

STATUS OF DEVELOPMENT OF THE LSA-SAF EVAPOTRANSPIRATION PRODUCT

F. Gellens-Meulenberghs, A. Arboleda and N. Ghilain

Department Research and Development, Royal Meteorological Institute
Avenue Circulaire, 3, B-1180 Brussels, Belgium

ABSTRACT

An evapotranspiration (ET) algorithm is currently developed by the LSA-SAF. An experimental version is running in real time at the LSA-SAF Host Institute since February 2005. It uses MSG derived LSA-SAF input (DSSF, DSLF, LST and AL) and ECMWF meteorological forcing to generate hourly ET maps over Europe. A drawback of this version is that it needs LST as a mandatory input and that this variable is not generated neither for areas with clouds nor for northern latitudes. A new variant of the algorithm is described that allows the generation of ET results for each pixel of the European window. Inclusion in a further version of other LSA-SAF input data (related to vegetation and snow) is in preparation. To answer to a recommendation of the Review Board, the firstly used IGBP land cover database can now be replaced into the developed software by a database derived from ECOCLIMAP-1. Maps are presented to illustrate the results.

Validation is the main activity of the ET team during the IOP phase. Different aspects will be presented and discussed. Off-line comparisons have been done with observations of a large sample of flux stations, mainly located in Europe. The LSA-SAF ET results are also compared with the output from the ECMWF GCM, the Aladin LAM and GLDAS. Results of sensitivity studies are also summarized.

Future work includes the extension of the current application outside of Europe and the adaptation of the ET software to the processing of EPS derived data. Validation activities will be extended to northern latitudes and to the southern sparsely vegetated and arid areas where good quality validation data can be found.

1. INTRODUCTION

The evapotranspiration (ET) is an important term of the hydrological cycle. It includes both the contributions of the evaporation of the soil and the transpiration of the vegetation. The associated energy flux is called the latent heat flux [W m^{-2}]

$$LE = L_V E$$

with L_V the latent heat of vaporisation (L_V ~ 2,5 10^6 J kg^{-1}) and E is the evaporation flux [kg m^{-2} s^{-1}]. The ET process is thus involved in both the water cycle and the energy budget.

The Royal Meteorological Institute (RMI) of Belgium is a member of the LSA-SAF Project Team. Its objective in this framework is to conceive and develop an algorithm for the estimation of ET taking advantage of the improved capabilities of the new MSG and EPS sensors. The developments and results presented below are obtained by using MSG derived data over Europe.

2. METHODOLOGY

The developed method to assess ET, considers first sub-grid (or sub-pixel) homogeneous entities called 'tiles' and then the aggregation of the results obtained for the different tiles to obtain ET averaged values at pixel level. The different possible tile types (grassland, crops, forests, bare soil, …) and the respective fraction of coverage *?i* are deduced from a land cover database for each MSG pixel.

The method is an adaptation for remote sensing (e.g. Arboleda et al., 2005) of the ECMWF Tessel SVAT model (Viterbo and Beljaars, 1995; van den Hurk, et al., 2000). At tile level, the surface energy budget is expressed by

$$Rn - H_i - LE_i - G_i = 0$$

where H_i, LE_i, and G_i are respectively the sensible heat flux, the latent heat flux and the ground heat flux and Rn is the net radiation at the surface

$$Rn = (1-a)S_{\downarrow} + e(L_{\downarrow} - s T_{sk,i}^4)$$

In this expression a is the albedo (AL), $S?$ is the downwelling short wave surface flux (DSSF), e is the emissivity (EM), $L?$ is the donwelling surface longwave flux (DSLF), s is the Stefan-Boltzmann constant and T_{sk} is the skin temperature.

The sensible and latent heat fluxes are respectively computed as

$$H_i = \frac{r_a}{r_a}\left[c_p(T_{sk,i} - T_a) - gz_a\right]$$

and

$$LE_i = \frac{L_v r_a}{(r_a + r_c)}\left[q_{sat}(T_{sk,i}) - q_a(T_a)\right]$$

with $?_a$ the air density, r_a the aerodynamic resistance, c_p the heat capacity at constant pressure, T_a the air temperature height z_a, g is the acceleration due to gravity, r_c is the canopy or stomatal

resistance, q_a is the air specific humidity at level z_a, q_{sat} is the value of the surface specific humidity at saturation. The canopy resistance is computed following the Jarvis (1976) approach.

From the last two equations we see that T_{sk} corresponds to the aerodynamic temperature at tile level.

The method of Chehbouni (1996) is adopted here to deduce G_i from the Leaf Area Index (LAI) at tile level.

The averaged *H* and *LE* fluxes at pixel level are given by

$$H = \sum V_i H_i$$

and

$$LE = \sum V_i LE_i$$

The evapotranspiration at pixel level can directly be deduced from this latter equation.

3. INPUT DATA

In this version of the model, three variables (AL, DSSF an DSSF) derived from MSG by the LSA-SAF with hourly and full spatial resolution are used. The other meteorological input comes from the analysis and forecasts of the ECMWF model. As mentioned below, two land cover databases are considered: IGBP (Loveland et al., 1997) and ECOCLIMAP-1 (Masson et al., 2003). The IGBP database was adopted at first in the LSA-SAF while migration towards ECOCLIMAP has been recommended for future developments.

Besides the application of the algorithm with MSG input, validation tests have also been made with ground measurements used as input (see section 5).

4. APPLICATION

A first version of the ET algorithm has been implemented in the LSA-SAF system for test since February 2005. A drawback of this version is that it needs Land Surface Temperature (LST) as a mandatory input and that this variable is not generated neither for areas with clouds nor for northern latitudes. An improved version, presented here, has been developed in 2005. It allows the generation of ET results for each pixel of the European window.

The Figure 1 shows the result obtained over Europe for the 10th June 2005 at 12 UT by using either the ECOCLIMAP data base (on the left) or the former IGBP data base (on the right). The main differences can be observed over Eastern countries, in the Southern part of Scandinavia and in some places of the Iberian peninsula.

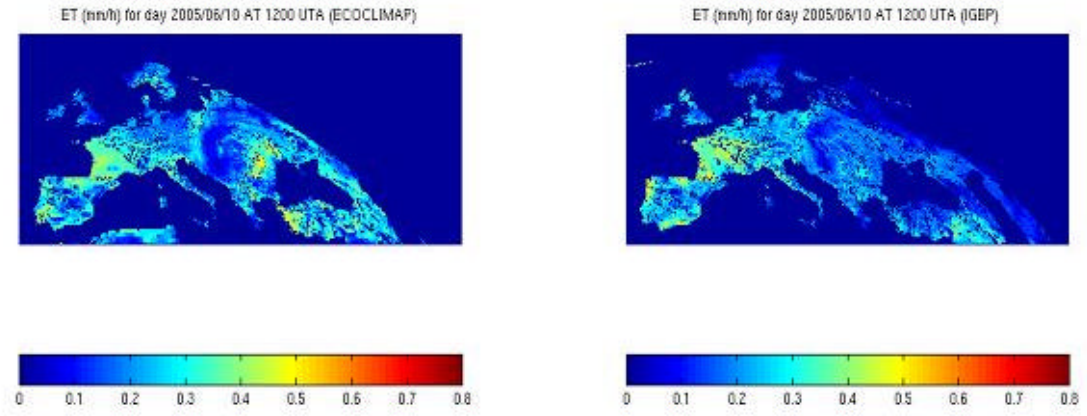

Figure 1: Comparison of ET maps, in mm/h, over Europe obtained for the 10th June 2005 by using ECOCLIMAP (left) or IGBP (right).

Different by-products can be derived from the full temporal ET product. The Figure 2 displays daily ET results obtained by temporal integration for two days in June 2006.

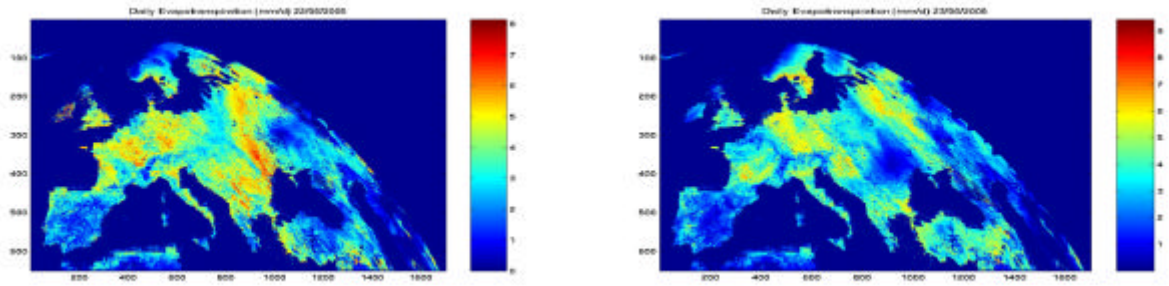

Figure 2: Daily ET results (mm) obtained by temporal integration for the 22nd and 23rd June 2005

The fraction of evaporation is defined as the proportion of the available energy at the surface consumed by the ET process. It is given by

$$f_{EV} = \frac{LE}{Rn - G} = \frac{LE}{LE + H}$$

This variable can be viewed as a soil wetness or soil aridity index. Indeed, it increases in well-watered conditions and decreases with the occurrences of droughts. An example is presented at the Figure 3 for the 22th June 2005.

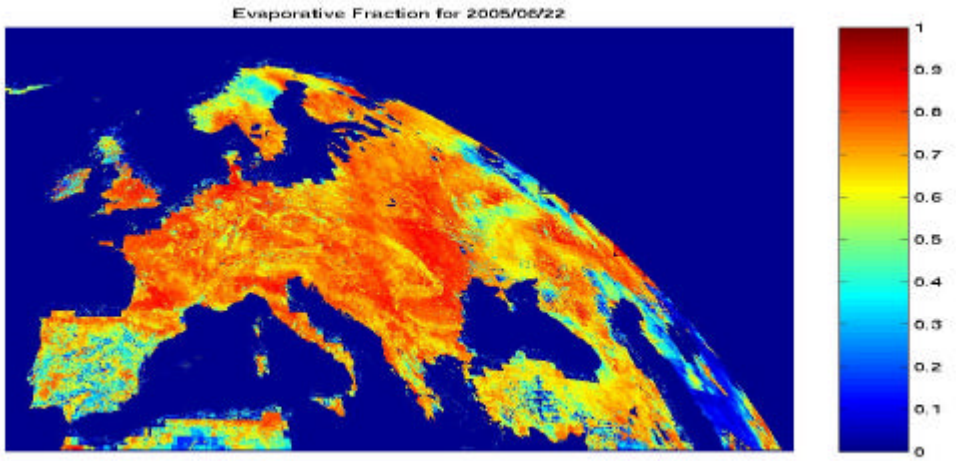

Figure 3: Map of the fraction of evaporation calculated for the 22nd June 2005

5. VALIDATION

Validation is the main activity of the ET team during the IOP phase. We achieved comparison, in one hand, with time series of ground stations data and, in the other hand, with results from short range forecast from ECMWF and from GLDAS. Validation has been performed on LSA-SAF ET by two different approaches.

The first approach to validate the ET results is to compare with measured values at local scale, i.e. at ground stations. A period of time of 18 days in June 2005 has been chosen to perform the comparison at different sites in Europe and on different biomes. The stations involved in this exercise are either part of national weather services network or part of the European network CarboEurope/Euroflux (Aubinet et al., 2000). For this part of validation, a strong selection of candidate measurement stations has been applied to keep only stations where the underlying vegetation is homogeneous over a sufficient area. This criterion is very important while performing comparisons in order to ensure that the measurements are representative of their environment. This choice has been performed by contacts with investigators of stations. The figure 4a represents a time series comparison of results from LSA-SAF ET with reference values produced by RMI at the station Melle over grass, in Belgium. An other comparison is shown in figure 4b, where model results are confronted to the measurements made over a Mediterranean forest in Puéchabon, in South of France. Estimated values of evapotranspiration by LSA-SAF ET fit well the stations values at a time step of 30 minutes. Gaps in LSA-SAF ET time series are mainly due to missing input variables. Differences between versions using IGBP or ECOCLIMAP are noticed at Melle station. Comparisons are currently pursued over a large range of climate conditions and biomes to validate further our estimations and to check the positive effect of introducing ECOCLIMAP in LSA-SAF ET.

The second way adopted to validate is to compare images of LSA-SAF ET results with outputs of ECMWF model and GLDAS (Rodell et al., 2004). At this stage, short-range forecasts of evapotranspiration from both systems have been used for comparison, at a three-hourly time step. We compared these images to the three-hourly averages of LSA-SAF ET at the MSG resolution. In Figure 5, images over Europe from the three systems are shown for a particular time steps for the 22nd of June 2005, accompanied by frequency histogram of the ET values.

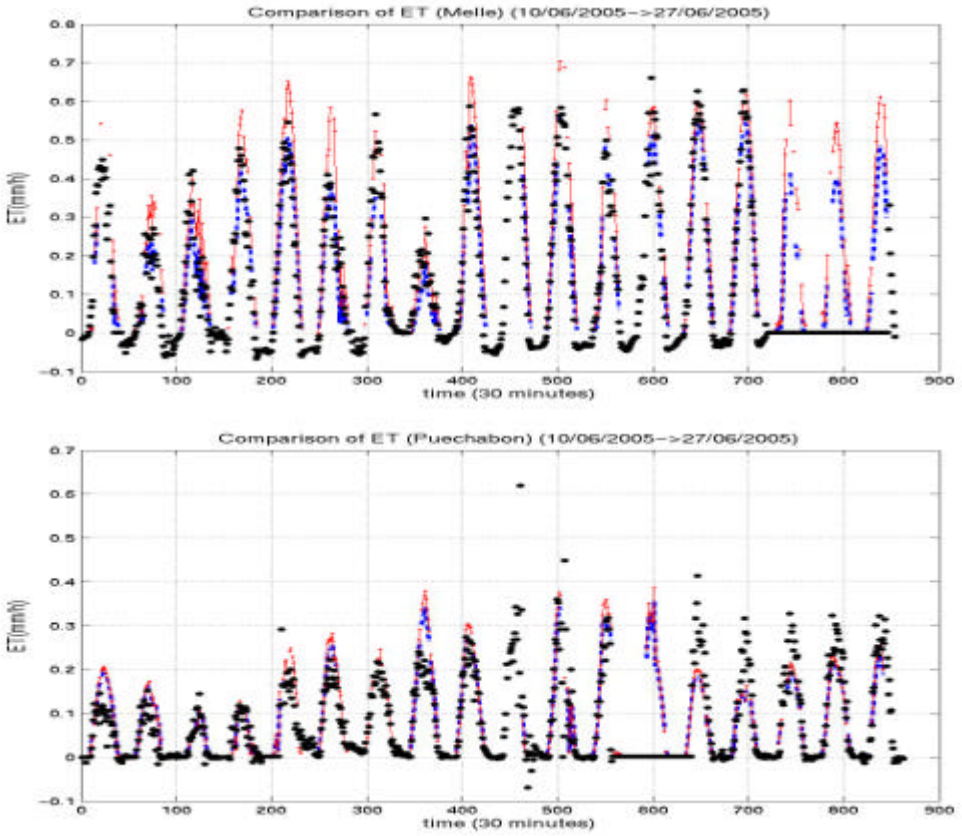

Figure 4: Time series comparison of ET, in mm/h, for two sites. ET results with IGBP is the dash-dotted line, ET results with ECOCLIMAP are represented by the thin line and, finally, the dots are the reference values at the stations. a) comparison at the Melle meteorological station in Belgium; b) comparison at Puéchabon flux tower site in South of France.

A quick look at the images and distribution gives an idea of the striking difference between ECMWF forecasts and GLDAS outputs. In comparison, as we expected, maps from LSA-SAF ET are found closer to ECMWF forecasts than to GLDAS outputs. Although the raison why there is a difference with GLDAS is not explained, we suspect that the similarity we observed with ECMWF is due to the use of ECMWF soil moisture forecasts in our algorithm, while GLDAS uses a different way of predicting this variable. The difference is patent for example for Iberian peninsula where GLDAS gives very low evapotranspiration compared to the two other systems.

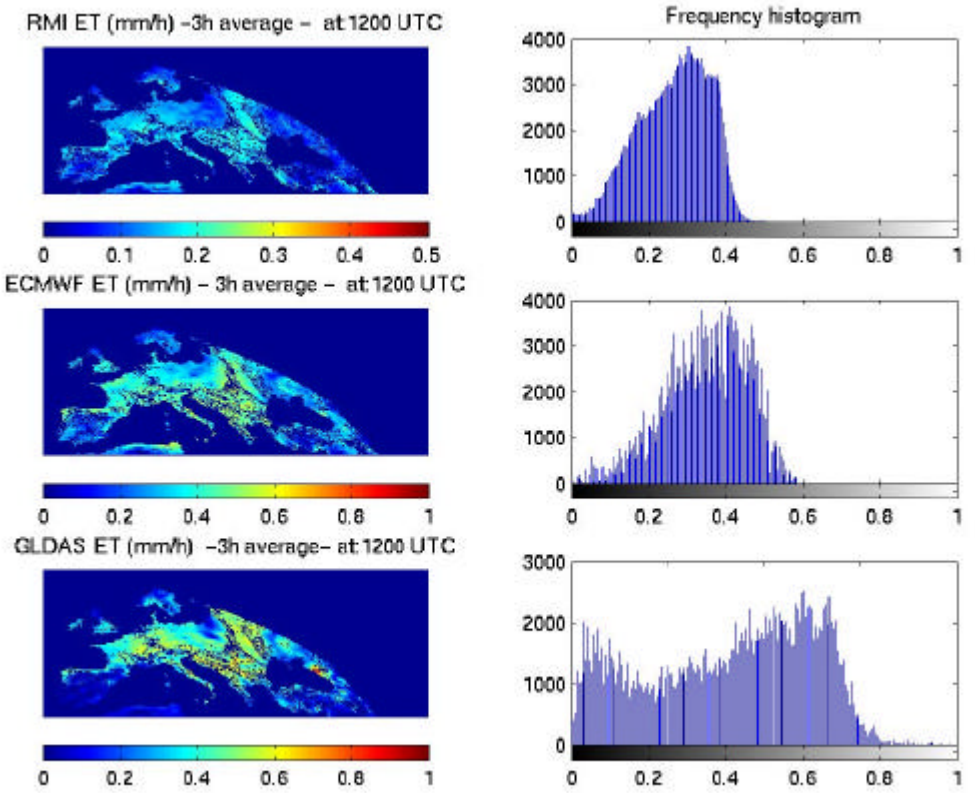

Figure 5: Left: Comparison of three-hourly averaged ET (mm/h) images over Europe from LSA-SAF ET, ECMWF and GLDAS for 12UTC the 22nd of June 2005. Right: Comparison of the ET frequency histogram for the three images.

	DSSF	DSLF	ALBEDO
RMSE	15W/M² (CLEAR SKY)	10%	10%

Table 1: Root mean square error (RMSE) of LSA-SAF product as specified in the User Requirement Document.

To complete the work of validation, we also performed an algorithm sensitivity study to errors from input LSA-SAF products, i.e. AL, DSSF and DSLF. For the sensitivity test, a probabilistic approach has been chosen, assuming the error of input variables is normally distributed, using as standard deviation the error specified for each product in the User Requirement Document (see table 1). 5000 runs of ET model are performed and resulting ET distribution for each time step is compared to a control run. The test is performed for a period of 12 days (19-30 June 2005) at Cabauw (The Netherlands), using measured radiation components.

The induced error found on ET exhibits a diurnal cycle pattern as well for the absolute error, i.e. standard deviation, than for the relative error. Figure 6 shows both relative and absolute error induced by combined uncertainties of the three inputs from LSA-SAF. Minimum relative error is found around solar noon, i.e. between 5% and 10%, corresponding the maximum of absolute error. In contrast, high relative error is found for early morning and late afternoon, but corresponds the lowest absolute errors.

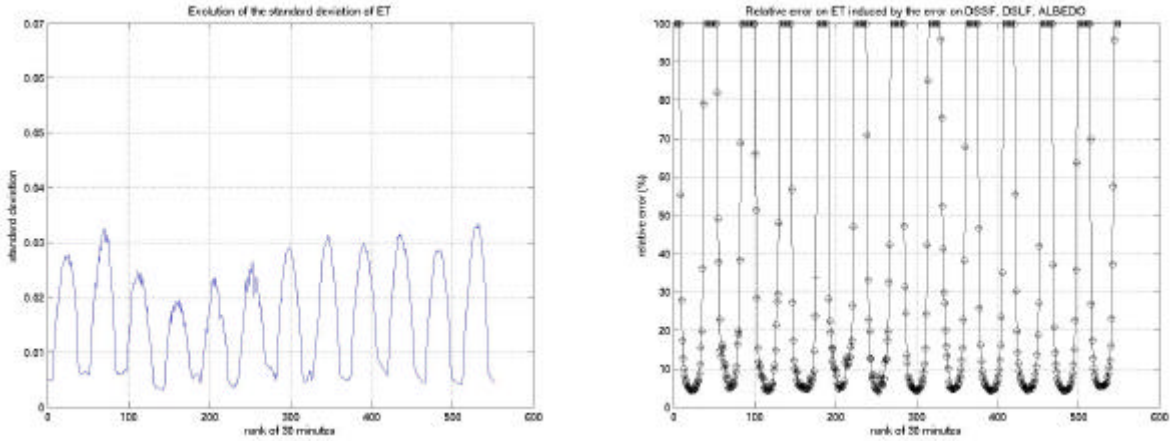

Figure 6: Left: Absolute error (mm/h) induced on ET results by uncertainty in the input LSA-SAF variables. Right: Relative error (%) induced on ET results by uncertainty in the input LSA-SAF variables.

This fact is also confirmed when relative error is plotted in function of the solar radiation at the surface, i.e. DSSF, as shown in Figure 7. For midday values, LSA-SAF ET is only slightly sensitive to input errors, i.e. 5%-10%. However, for small values of incident solar radiation relative error increases.

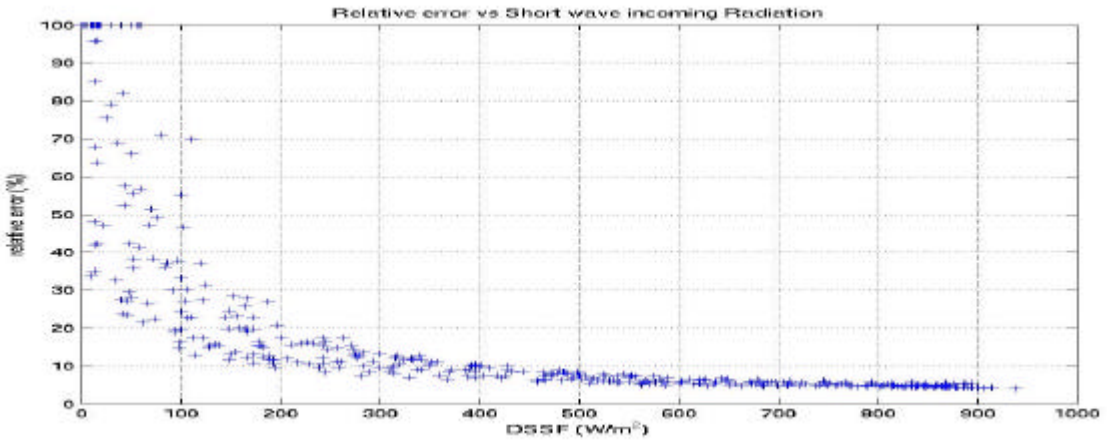

Figure 7: Relative error (%) induced on ET results by uncertainty in the input LSA-SAF variables plotted in function of solar incident radiation at surface (DSSF).

This sensitivity study has been pursued to evaluate the sensitivity to meteorological forcings, like air temperature, wind and air humidity.

6. DEVELOPMENTS PLANNED FOR 2006

The current version of the ET uses three LSA-SAF variables as input: DSSF, DSLF and AL. Tests will be made in 2006 in order to evaluate the improvements of the results obtained by introducing more satellite derived input like the emissivity (EM), the snow cover (SC), the fraction of vegetation (FVC) and the leaf area index (LAI). Tests will be made by comparison of ET results in a subset of ground stations. If they appear to be conclusive, a new version of the algorithm will be achieved.

Research is needed to determine how the radiative land surface temperature (LST) can be used to improve the aerodynamic temperature (Tskin). These two temperatures correspond to different physical concepts. Moreover, as the other LSA-SAF results, LST is available at the pixel spatial resolution whereas the ET model computes Tskin at tile level. LST is only available for clear sky cases and Southern latitudes. A first test has been made at the Evora station (Portugal) and shows large differences between LST and Tskin.

In the current version of the ET algorithm, ECMWF SM input is used and good results are obtained in most cases over Europe. Comparison between observed and ECMWF SM showed large differences at some investigated stations (Evora in Portugal and El Saler in Spain). We conclude that the ET algorithm requires an adapted SM index. This latter can probably be scaled from true physical SM observations or future satellite derived data.

Furthermore, preliminary tests have showed that at least in some cases, an assimilation of LST in the ET algorithm is able to improve SM and ET.

7. FUTURE WORK (CDOP)

During the next phase (CDOP), all LSA-SAF products, including ET and SM, should be generated on the full MSG disk. The validation of the ET model should be extended to Southern regions with arid, semi-arid and tropical climate conditions (Africa and a part of South America). The best available datasets will be searched. AMMA datasets are of particular interest (Boone, 2006). Comparisons with FLUXNET / CarboEurope observations will be pursued. The new possibilities offered by scintillometry (e.g. Kohsiek et al., 2002; Beyrich et al., 2002 and de Bruin, 2006) to validate H will be investigated depending of data availability. Improvements of the methodology will be introduced if necessary as a function of the validation results.

Special attention will be paid to the optimal use of vegetation parameters, LST and SM in view to consolidate or improve the ET results. In particular, more research is needed to develop, in the LSA-SAF, coherent ET and SM products based on satellite data. The first METOP satellite of the EUMETSAT Polar System (EPS) should be launched in 2006. H-SAF (Bizzarri, 2006; Wagner, 2006) intends to derive surface SM from microwave measurements while assimilation techniques should be used to derive SM profiles. Collaboration between LSA-SAF and H-SAF are planned during the CDOP in the framework of interSAF activities.

8. CONCLUSIONS

- First ET software has been implemented for test in the LSA-SAF system since February 2005 and generates ET results in real time. An improved version, developed and extensively tested in 2005, will be implemented soon. This new version can use either the IGBP or the ECOCLIMAP data bases.

- More research is planned in the future to develop a LSA-SAF SM index derived from satellite observations. However, as satisfying results are obtained right now over Europe with ECMWF SM, we suggest that ET can be run operationally using ECMWF SM as a first step.

- RMI is ready to participate actively during CDOP to the development of a LSA-SAF SM product able to improve ET results.

- ET is generated with full MSG spatial and temporal resolution. In the future additional products could be provided to satisfy users requests. For example daily integrated maps of ET, or fraction of evaporation, can easily be derived from the full temporal resolution output.

9. ACKNOWLEDGMENTS

We thank all data flux providers contacted: S. Rambal, A. Carrara, F. Bosveld, J.C. Calvet, M. Aubinet, A. Wolfgang, B. Longdoz, L. Montagnani, R. Ceulemans, A. Granier, H. Verbeeck, M. Marek and P. Cellier, hopping that nobody has been missed in this list. We also acknowledge suggestions made by R. Stockli, M. Rodell, H. Kato and LSA-SAF colleagues for discussions.

We owe complementary funding of this project to ESA and Belgian Science Policy (ESA/Contract Nr. 15066/01/NL/Sfe(IC)).

10. REFERENCES

ARBOLEDA, A., GHILAIN, N. and GELLENS-MEULENBERGHS, F., (2005) The LSA-SAF evapotranspiration product - first results with MSG. Proceedings of the 2005 EUMETSAT meteorological satellite data user's conference, Dubrovnik, Croatia, 19th - 23th September 2005, 7 pp.

AUBINET, M., GRELLE, A., IBROM, A., RANNIK, U., MONCRIEFF, J., FOKEN, J., KOWALSKI, A.S., MARTIN, P.H., BERBIGIER, P., BERNHOFER, Ch., CLEMENT, R., ELBERS, J., GRANIER, A., GRUNSWALD, T., MORGENSTERN, K., PILEGAARD, K., REBMANN, C., SNIJDERS, W., VALENTINI, R. and VESALA T., (2000), Estimates of the net Annual Net Carbon and Water Exchanges of Forests: The EUROFLUX Methodology, Advances in ecological research, 30, pp.113-175.

BEYRICH, F., DE BRUIN, H. A. R., MEIJNINGER, W. M. L., SCHIPPER, J. W. and LOHSE, H., (2002) Results from one-year continuous operation of a large aperture scintillometer over a heterogeneous land surface. Boundary-Layer Meteorol., 105, pp. 85-97.

BIZZARRI, B., (2006) The EUMETSAT Satellite Application Facility on support to Operational Hydrology and Water Management (H-SAF). Proceedings of the 2nd LSA-SAF Training Workshop, Lisbon, Portugal, 8-10 March (this issue).

BOONE, A., (2006) The use of LAND SAF flux products in the AMMA Project. Proceedings of the 2nd LSA-SAF Training Workshop, Lisbon, Portugal, 8-10 March (this issue).

CHEHBOUNI, A., QI, J., LO SEEN, D., KERR, Y. H., DEDIEU, G., MORAN, S., DAUBAS, M. and MONTENY, B. M. (1996) Estimation of real evaporation. Proceedings of the international workshop on remote sensing and water resources, Montpellier, 30 November 1995, 10 pp.

DE BRUIN, H., (2006) Actual evaporation, sensible heat flux and reference crop evapotranspiration as potential new Land SAF products. Proceedings of the 2nd LSA-SAF Training Workshop, Lisbon, Portugal, 8-10 March (this issue).

JARVIS, P. G., (1976) The interpretation of the variations in leaf water potential and stomatal conductance found in canopies in the field. Phil. Trans. Roy. Soc. London, B273, pp. 593-610.

KOHSIEK, W., MEIJNINGER, W. M. L., MOENE, A. F., HEUSINKVELD, B. G., HARTOGENSIS, O. K., HILLEN, W. C. A. M. and DE BRUIN, H. A. R., (2002) An extra large aperture scintillometer for long range application. Boundary-Layer Meteorol., 105, pp. 119-127.

LOVELAND, T. R. and BELWARD, A. S., (1997) International Journal of Remote Sensing, v. 18, no. 5, p. 3,289-3,295, The IGBP-DIS Global 1 km Land Cover Data Set, DISCover First Results.

MASSON, V., CHAMPEAUX, J.L., CHAUVIN, F., MERIGUET, Ch. and LACAZE, R. A., (2003) Global Database of Land Surface Parameters at 1-km Resolution in Meteorological and Climate Models. Journal of Climate 16(9): 1261-1282

RODELL, M., HOUSER, P.R., JAMBOR, U., GOTTSCHALCK, J., MITCHELL, K., MENG, C.-J., ARSENAULT, K., COSGROVE, J., RADAKOVITCH, J., BOSILOVICH, M., ENTIN, J.K., WALKER, J.P., LOHMANN, D. and TOLL, D., (2004) The Global Land Data Assimilation System, Bull. Amer. Meteor. Soc., 85 (3), pp. 381-394.

VAN DEN HURK, B., VITERBO, P., BELJAARS, A., BETTS, A., (2000) Offline validation of the ERA40 surface scheme. ECMWF Technical Memorandum No.295, 42 pp.

VITERBO, P. and BELJAARS, A, (1995) An improved surface parametrization scheme in the ECMWF model and its validation, J. Climate, 8, pp. 2716-2748.

WAGNER, W., (2006) Soil moisture: synergistic approach for the merge of thermal and ASCAT information. Proceedings of the 2nd LSA-SAF Training Workshop, Lisbon, Portugal, 8-10 March (this issue).